



저작자표시-비영리-동일조건변경허락 2.0 대한민국

이용자는 아래의 조건을 따르는 경우에 한하여 자유롭게

- 이 저작물을 복제, 배포, 전송, 전시, 공연 및 방송할 수 있습니다.
- 이차적 저작물을 작성할 수 있습니다.

다음과 같은 조건을 따라야 합니다:



저작자표시. 귀하는 원저작자를 표시하여야 합니다.



비영리. 귀하는 이 저작물을 영리 목적으로 이용할 수 없습니다.



동일조건변경허락. 귀하가 이 저작물을 개작, 변형 또는 가공했을 경우에는, 이 저작물과 동일한 이용허락조건하에서만 배포할 수 있습니다.

- 귀하는, 이 저작물의 재이용이나 배포의 경우, 이 저작물에 적용된 이용허락조건을 명확하게 나타내어야 합니다.
- 저작권자로부터 별도의 허가를 받으면 이러한 조건들은 적용되지 않습니다.

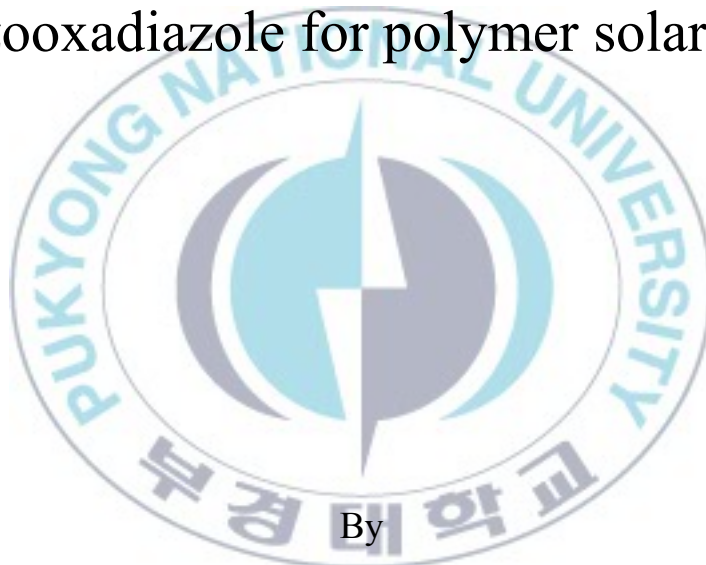
저작권법에 따른 이용자의 권리는 위의 내용에 의하여 영향을 받지 않습니다.

이것은 [이용허락규약\(Legal Code\)](#)을 이해하기 쉽게 요약한 것입니다.

[Disclaimer](#)

Thesis for the Degree of Master of Engineering

Synthesis and photovoltaic properties of π -
conjugated polymers based on
benzimidazole, arylene imide and
benzooxadiazole for polymer solar cells



By

Do Thu Trang

Department of Polymer Engineering

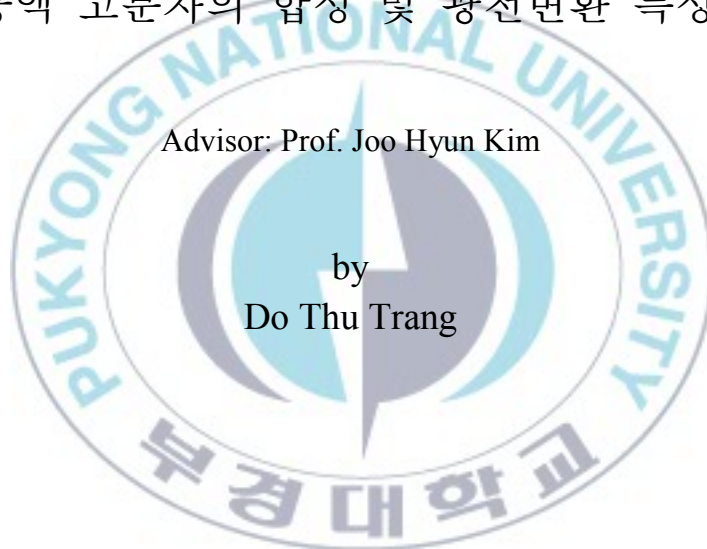
The Graduate School

Pukyong National University

February 2013

Synthesis and photovoltaic properties of π -
conjugated polymers based on
benzimidazole, arylene imide and
benzooxadiazole for polymer solar cells

(고분자 태양전지를 위한 벤즈이미다졸,
아릴렌이미드 및 벤즈옥사디아졸을 본골격으로하는
공액 고분자의 합성 및 광전변환 특성)



Advisor: Prof. Joo Hyun Kim

by
Do Thu Trang

A thesis submitted in partial fulfillment of the requirements
for the degree of

Master of Engineering

in Department of Polymer Engineering,
The Graduate School, Pukyong National University

February 2013

Synthesis and photovoltaic properties of π -conjugated polymers based
on benzimidazole, arylene imide and benzooxadiazole for polymer
solar cells

A dissertation

by

Do Thu Trang

Approved by:

(Seong-II Yoo)

(Won-Ki Lee)

(Joo Hyun Kim)

February 24, 2013

Contents

Contents	I
List of Figures	VIII
List of Tables	X
List of Schemes	XI
Abstract	XII

Chapter I. Introduction

1

I-1. Basic processes in organic solar cells (OSCs)	1
I-1-1. Absorption of photons	3
I-1-2. Exciton diffusion	3
I-1-3. Charge separation	4
I-1-4. Charge transport	4
I-1-5. Charge collection	5
I-2. Device Architecture	5
I-2-1. Single layer	5

I-2-2. Bilayer heterojunction	6
I-2-3. Bulk heterojunction (BHJ)	6
I-2-4. Diffuse bilayer heterojunction	7
I-3. Donor and acceptor materials for OSCs	9
I-3-1. Donor (p-type material)	9
I-3-2. Acceptor (n-type material)	10
I-4. Solar cell parameters	12
I-4-1. Open circuit voltage (V_{oc})	12
I-4-2. Short-circuit current (J_{sc})	14
I-4-3. Fill factor (FF)	14
I-4-4. Incident photon to current efficiency (IPCE)	16
I-4-5. Power conversion efficiency (η_p)	16
I-5. Factors affect the efficiency of OSCs	17
I-5-1. Solvent, concentration and active layer thickness	17
I-5-2. Ratio between polymer and fullerene	19
I-5-3. Annealing temperature	19
I-5-4. Molecular weight	20
I-5-5. Processing additives	21

I-5-6. Other factors	22
I-6. Low Band gap Polymers	23
Chapter II. Synthesis and Characterization of π-Conjugated Polymers Based on 2-Arylbenzimidazole and 4,7-Di-2-thienyl-2,1,3-benzothiadiazole	27
II-1. Introduction	27
II-2. Experimental Section	28
II-2-1. Materials and Synthesis	28
II-2-1-1. 3,6-Dibromo-benzene-1,2-diamine (1)	28
II-2-1-2. 4,7-Dibromo-2-(4- <i>tert</i> -butyl-phenyl)-1 <i>H</i> -benzoimidazole (2)	29
II-2-1-3. 4,7-Dibromo-2-(4- <i>tert</i> -butyl-phenyl)-1-ethyl-1 <i>H</i> -benzoimidazole (3)	30
II-2-1-4. 2-(4- <i>tert</i> -butyl-phenyl)-1-ethyl-4,7-di-thiophen-2-yl-1 <i>H</i> - benzoimidazole (4)	31

II-2-1-5. 4,7-Bis-(5-bromo-thiophen-2-yl)-2-(4- <i>tert</i> -butyl-phenyl)-1-ethyl- 1 <i>H</i> -benzimidazole (5)	32
II-2-1-6. Synthesis of Polymers POFTBT-IMD	33
II-2-2. Measurement	35
II-3. Results and Discussion	36
II-3-1. Thermal Properties	36
II-3-2. Optical Properties	38
II-3-3. Electrochemical Properties	40
II-4. Conclusions	42
Chapter III. Synthesis and Characterization of π-Conjugated Polymer Based on Arylene Imide for Organic Solar Cells	43

III-1. Introduction	43
III-2. Experimental Section	46

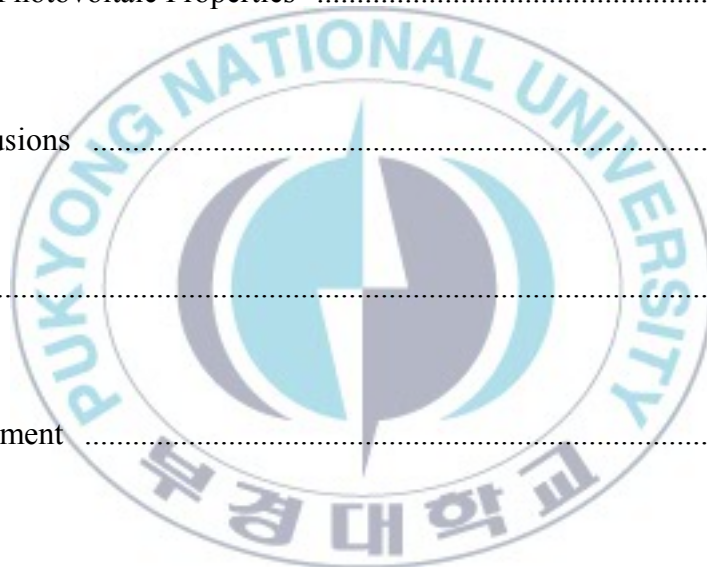
III-2-1. Materials and Synthesis	46
III-2-1-1. 1,2-Bis-decyloxy-benzene (1)	47
III-2-1-2. 1,2-Diiodo-4,5-bis-decyloxy-benzene (2)	48
III-2-1-3. 1,2-Dicyano-4,5-bis-decyloxy-benzene (3)	49
III-2-1-4. 4,5-Bis-decyloxy-phthalic acid (4)	50
III-2-1-5. 2-Butyl-5,6-bis-decyloxy-isoindole-1,3-dione (5)	51
III-2-1-6. 4,7-Dibromo-2-butyl-5,6-bis-decyloxy-isoindole-1,3-dione (6)	52
III-2-1-7. 2-Butyl-5,6-bis-decyloxy-4,7-di-thiophen-2-yl-isoindole-1,3-dione (7)	53
III-2-1-8. 4,7-Bis-(5-bromo-thiophen-2-yl)-2-butyl-5,6-bis-decyloxy-isoindole-1,3-dione (8)	54
III-2-1-9. Synthesis of Polymer T-TI24T	55
III-2-2. Fabrication of Device	57
III-2-3. Measurement	58
III-3. Results and Discussion	59
III-3-1. Thermal Properties	59
III-3-2. Optical Properties	61
III-3-3. Electrochemical Properties	63
III-3-4. Photovoltaic Properties	65

III-4. Conclusion	68
-------------------------	----

Chapter IV. Synthesis, Characterization and photovoltaic properties of π -Conjugated Polymers Based on Thiophene and 2,1,3-Benzoxadiazole Derivatives for Organic Solar Cells69

IV-1. Introduction	69
IV-2. Experimental Section	73
IV-2-1. Materials and Synthesis	73
IV-2-1-1. 1,2-Dinitro-4,5-bis-decyloxy benzene (3)	73
IV-2-1-2. 5,6-Bis(decyloxy)benzo[c][1,2,5]oxadiazole (4)	74
IV-2-1-3. 4,7-Dibromo-5,6-bis(decyloxy)benzo[c][1,2,5]oxadiazole (5)	75
IV-2-1-4. 5,6-Bis(decyloxy)-4,7-di(thien-2-yl)benzo[c][1,2,5]oxadiazole (6)	76
IV-2-1-5. 4,7-Bis(5-bromothien-2-yl)-5,6-bis(decyloxy)benzo[c][1,2,5]oxadiazole (7)	77
IV-2-1-6. Synthesis of polymers (1T-BO20, 2T-BO20 and 3T-BO20)	78
IV-2-2. Fabrication of Device	80

IV-2-3. Measurement	81
IV-3. Results and Discussion	82
IV-3-1. Thermal Properties	82
IV-3-2. Optical Properties	84
IV-3-3. Electrochemical Properties	87
IV-3-4. Photovoltaic Properties	91
IV-4. Conclusions	100
References	101
Acknowledgment	106



List of Figures

Figure I-1. The operating principle of bulk heterojunction type OSC.

Figure I-2. The structures of OSCs:

(a) Single layer; (b) Bilayer heterojunction; (c) Bulk heterojunction.

Figure I-3. Donor and acceptor materials for OSCs.

Figure I-4. Energy level alignment at the DA-interface.

Figure I-5. *J-V* curves with and without illumination of a typical solar cell device.

Figure I-6. Solar photon flux (the solid line) spectrum (AM 1.5G) and absorption spectrum of P3HT (the line with circles).

Figure I-7. Molecular orbital interactions of donor and acceptor units, resulting in a narrowing of the band gap in push-pull conjugated copolymers.

Figure II-1. TGA thermogram of polymers POTBT, POFTBT-IMD5 and POFTBT-IMD10 with a heating rate of $10\text{ }^{\circ}\text{C min}^{-1}$ under a N_2 atmosphere.

Figure II-2. Normalized UV-Vis absorption and Photoluminescence spectrum of POFTBT, POFTBT-IMD5 and POFTBT-IMD10.

Figure II-3. Cyclic voltammogram of POFTBT, POFTBT-IMD5 and POFTBT-IMD10.

Figure III-1. Chemical structures of copolymers based on arylene imide.

Figure III-2. TGA thermogram of polymer T-TI24T with a heating rate of 10 °C min⁻¹ under a N₂ atmosphere.

Figure III-3. UV-Vis absorption and PL spectrum of T-TI24T film.

Figure III-4. Cyclic voltammogram of T-TI24T in an MC:DCB (1:1 v/v) of 0.1 M Bu₄NPF₆.

Figure III-5. *J-V* curves of conventional type OSCs based on T-TI24T under the illumination of AM 1.5G, 100 mW/cm².

Figure III-6. *J-V* curves of conventional type OSCs based on T-TI24T under the dark condition.

Figure IV-1. Chemical structures of copolymers based on BO.

Figure IV-2. TGA thermogram of polymers 1T-BO20, 2T-BO20 and 3T-BO20 with a heating rate of 10 °C min⁻¹ under a N₂ atmosphere.

Figure IV-3. UV-Vis absorption spectra of 1T-BO20, 2T-BO20 and 3T-BO20 films.

Figure IV-4. Cyclic voltammogram of 1T-BO20, 2T-BO20 and 3T-BO20.

Figure IV-5. Energy level diagram of 1T-BO20, 2T-BO20 and 3T-BO20.

Figure IV-6. *J-V* curves of OSCs based on 1T-BO20, 2T-BO20 and 3T-BO20.

a) Under the illumination of AM 1.5G, 100 mW/cm²

b) Under the dark condition

Figure IV-7. *J-V* curves of OSCs based on 1T-BO20, 2T-BO20 and 3T-BO20 with 1% DIO.

- a) Under the illumination of AM 1.5G, 100 mW/cm²
- b) Under the dark condition

Figure IV-8. AFM height images of polymer:PC₆₁BM blend films: (a) 1T-BO20 without DIO; (b) 1T-BO20 with 1% DIO; (c) 2T-BO20 without DIO; (d) 2T-BO20 with 1% DIO; (e) 3T-BO20 without DIO; (f) 3T-BO20 with 1% DIO.



List of Tables

Table II-1. Optical absorption and electrochemical properties of POFTBT, POFTBT IMD5 and POFTBT IMD10.

Table III-1. Summary of band gaps, HOMO levels, and photovoltaic properties of conjugated polymers based on arylene imide.

Table III-2. Molecular weight and thermal properties of T-TI24T.

Table III-3. Optical absorption and electrochemical properties of T-TI24T.

Table III-4. Photovoltaic properties of T-TI24T.

Table IV-1. Summary of band gaps, HOMO levels, and photovoltaic properties of conjugated polymers based on BO.

Table IV-2. Molecular weight and thermal properties of 1T-BO20, 2T-BO20 and 3T-BO20.

Table IV-3. Optical absorption and electrochemical properties of 1T-BO20, 2T-BO20 and 3T-BO20.

Table IV-4. Photovoltaic properties of OSCs incorporating BO-based polymers.

List of Schemes

Scheme II-1. Synthesis of monomer and polymer (POFTBT-IMD).

Scheme III-1. Synthesis of monomer and polymer (T-TI24T).

Scheme IV-1. Synthesis of monomers and polymers (1T-BO20, 2T-BO20 and 3T-BO20).



Synthesis and photovoltaic properties of π -conjugated polymers based on benzimidazole, arylene imide and benzooxadiazole for polymer solar cells

Do Thu Trang

*Department of Polymer Engineering, The Graduate School
Pukyong National University*

요약

지난 10년 동안, 유기태양전지의 활성층으로 높은 전하 이동도를 가지는 regioregular poly(3-hexylthiophene) (rr-P3HT)가 많이 사용되었다. 그러나 rr-P3HT는 큰 band-gap을 가져 유기태양전지의 활성층으로 사용하기에 이상적인 물질이 아니다. 보다 많은 광자를 얻고, 에너지 준위를 조절하기 위한 시도 중의 하나는, main chain을 전자가 풍부한 unit (donor)과 전자가 부족한 unit (acceptor)을 이용하여 conjugated 형태의 공중합체를 합성하는 것이다.

본 논문에서, 2-aryl benzimidazole (IMD), arylene imide (TI24T), 또는 2,1,3-benzooxadiazole (BO20) 유도체를 acceptor로 사용하여 작은 band-gap을 가지는 고분자를 합성하였다. POFTBT-IMD는 2-aryl benzimidazole 유도체를 포함하는 4,7-dithiophen-2-yl-benzo(2,1,3)thiadiazole (TBT)와 높은 용해도를 가지는 fluorene 유도체를 Suzuki coupling 중합법으로 중합하였다. 또한 arylene imide/2,1,3-benzooxadiazole 유도체와 thiophene/dithiophene을 Stille coupling 중합법을 이용하여, T-TI24T, 1T-BO20, 2T-BO20, 3T-BO20를 중합하였다. 합성된 고분자는 chloroform, chlorobenzene, dichlorobenzene, toluene과 같은 일반적인 유기용매에 대해 우수한 용해도를 가지며, UV-Vis spectrum과 순환 전압 전류법 (cyclic voltammetry, CV)으로 1.6-2.3 eV 정도의 광학적, 전기화학적 band-gap을 가지는 것을 확인하였다. 그리고 비교적 낮은 호모 (low highest occupied molecular orbital, HOMO) 에너지 준위와 태양전지에 적용하기 적합한 에너지 준위를 가지는 것을 확인하였다. 합성된 T-

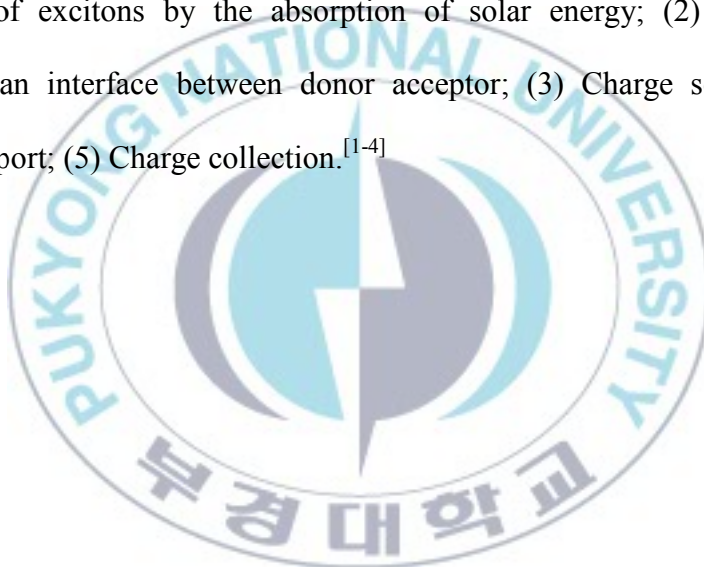
Ti24T, 1T-BO20, 2T-BO20, 3T-BO20를 bulk hetero junction (BHJ) 구조의 태양전지의 활성층으로 적용하여 소자를 제작하였다.



Chapter I. Introduction

I-1. Basic processes in organic solar cell (OSCs)

In general, for a successful OSC, five important processes have to be optimized to obtain a high conversion efficiency of solar energy into electrical energy: (1) Generation of excitons by the absorption of solar energy; (2) Diffusion of excitons to an interface between donor acceptor; (3) Charge separation; (4) Charge transport; (5) Charge collection.^[1-4]



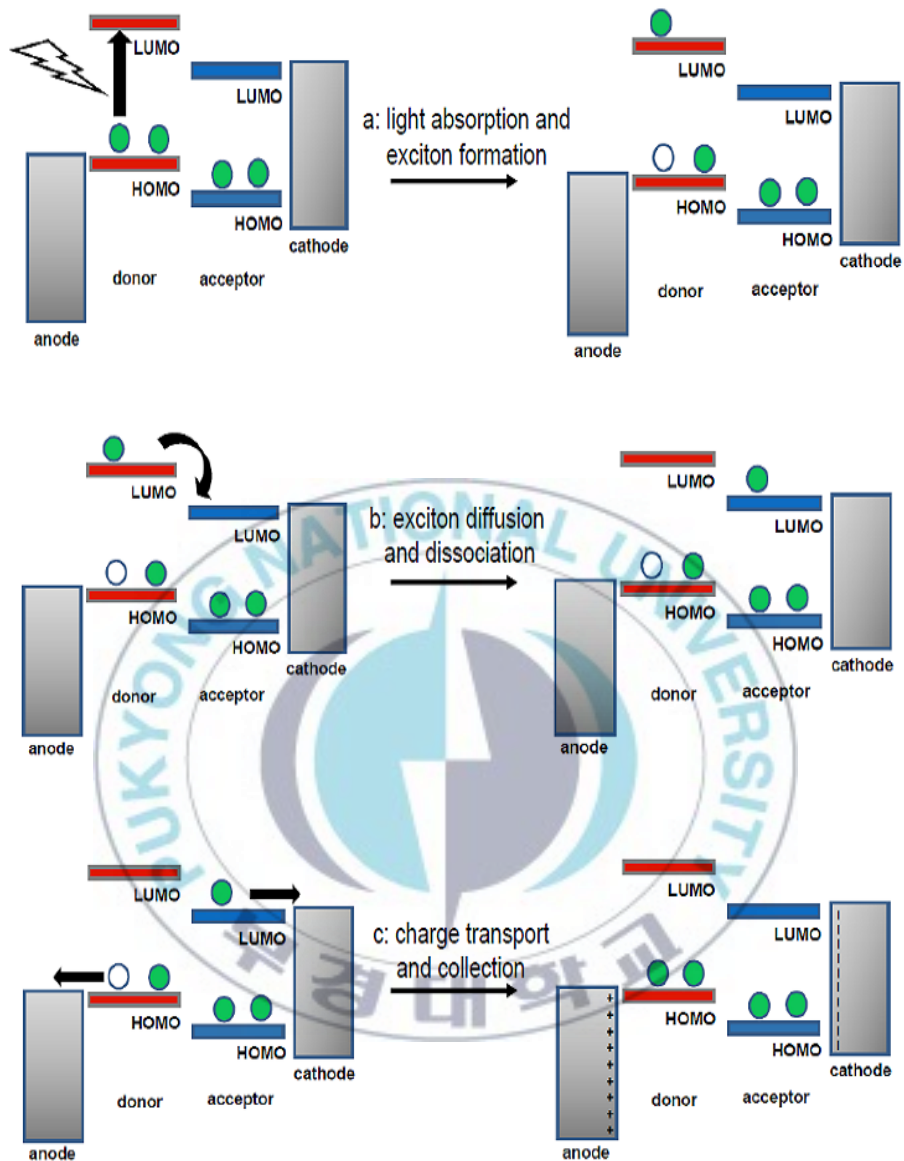


Figure I-1. The operating principle of bulk heterojunction type OSC.

I-1-1. Absorption of photons

In most of devices, very small portion of the incident light is absorbed for the following reasons:

- The band gaps of materials are too high. The majority of semiconducting polymer have band gaps higher than 2.0 eV (600 nm), which limit the absorption of the solar radiation.
- The organic layer is too thin. The typically low charge carrier and exciton mobility require layer thickness in the order of 100 nm. Fortunately the absorption coefficient of organic materials is generally much higher than Si so that only about 100 nm are necessary to absorb between 60 and 90% if a reflective back contact is used.

I-1-2. Exciton diffusion

Ideally, excitons should move to dissociation site. Since such a site may be at the other end of the semiconducting polymer, their diffusion length should be at least equal the required layer thickness (for sufficient absorption)-otherwise they recombine and photons were wasted. Exciton diffusion ranges in polymers and pigments are typically around 10 nm.

I-1-3. Charge separation

Charge separation occurs at the interface between donor and acceptor molecules. After photo-excitation of an electron from the highest occupied molecular orbital (HOMO) to the lowest unoccupied molecular orbital (LUMO), the electron can jump from the LUMO of the donor (the material with the higher LUMO) to the LUMO of the acceptor if the potential difference between the ionisation potential of the donor and the electron affinity of the acceptor is larger than the exciton binding energy. However, this process can lead to free charges only if the hole remains on the donor due to its higher HOMO level. In contrast, if the HOMO of the acceptor is higher, the exciton transfers itself completely to the material of lower band gap accompanied by energy loss.

I-1-4. Charge transport

The transport of charges is affected by recombination during the journey to the electrodes-particularly if the same material serves as transport medium for both electrons and holes. Also, interaction with atoms or other charges may slow down the travel speed and thereby limit the current.

I-1-5. Charge collection

The collection of charge carriers at the electrodes is regularly accomplished by a transparent conductive oxide such as ITO on one side and a relatively low work function metal (e.g. Al, Ca) on the other side. The contact of electrodes with the semiconductors will affect to this process. With the Ohmic contact, charges can easily reach electrodes whereas with blocking contact they cannot immediately enter.

I-2. Device Architecture

I-2-1. Single layer

The single layer device structure of OSC is comprised of a transparent electrode/organic photosensitive semiconductor/electrode. The structure is simple but absorption covering the entire visible range is rare using a single type of molecule. The photoactive region is often very thin and since both positive and negative photo-excited charges travel through the same material recombination losses are generally high.^[1,5,6]

I-2-2. Bilayer heterojunction

The bilayer OSC includes an additional electron transporting layer. This structure benefits from the separated charge transport layers that ensure connectivity with the correct electrode and give the separated charge carriers only little chance to recombine with its counterpart. The drawback is the small interface that allows only excitons of a thin layer to reach it and get dissociated.

I-2-3. Bulk heterojunction (BHJ)

The essence of the BHJ is to intimately mix the donor and acceptor components in a bulk volume so that each donor-acceptor interface is within a distance less than the exciton diffusion length of each absorbing site. The BHJ device is similar to the bilayer device with respect to the D-A concept, but it exhibits a largely increased interfacial area where charge separation occurs. Due to the interface being dispersed throughout the bulk, no loss due to too small exciton diffusion lengths is expected, because ideally all excitons will be dissociated within their lifetime. In this conception the charges are also separated within the different phases, and hence recombination is reduced to a large extent and the photocurrent often follows the light intensity linearly or slightly sub-linearly. Though in the bilayer heterojunction the donor and acceptor phase contact the anode and

cathode selectively, the BHJ requires percolated pathways for the hole and electron transporting phases to the contacts. In other words, the donor and acceptor phases have to form a bi-continuous and interpenetrating network. Therefore, the BHJ devices are much more sensitive to the nanoscale morphology in the blend.

I-2-4. Diffuse bilayer heterojunction

It is conceptually in between the bilayer and the BHJ device. This device structure is aiming to adapt the advantages of concepts, an enlarged donor–acceptor interface and a spatially uninterrupted pathway for the opposite charge carriers to their corresponding electrodes. The diffuse interface is achieved in different ways: (i) If processed from solution, two thin polymer films can be pressed together in a lamination procedure applying moderate pressure and elevated temperatures. (ii) Another way to achieve a diffuse interface is to spin coat the second layer from a solvent that partially dissolves the underlying polymer layer. (iii) Finally, also the controlled inter-diffusion between an acceptor fullerene and a donor polymer by annealing of a bilayer device results in an intermixed interfacial region.

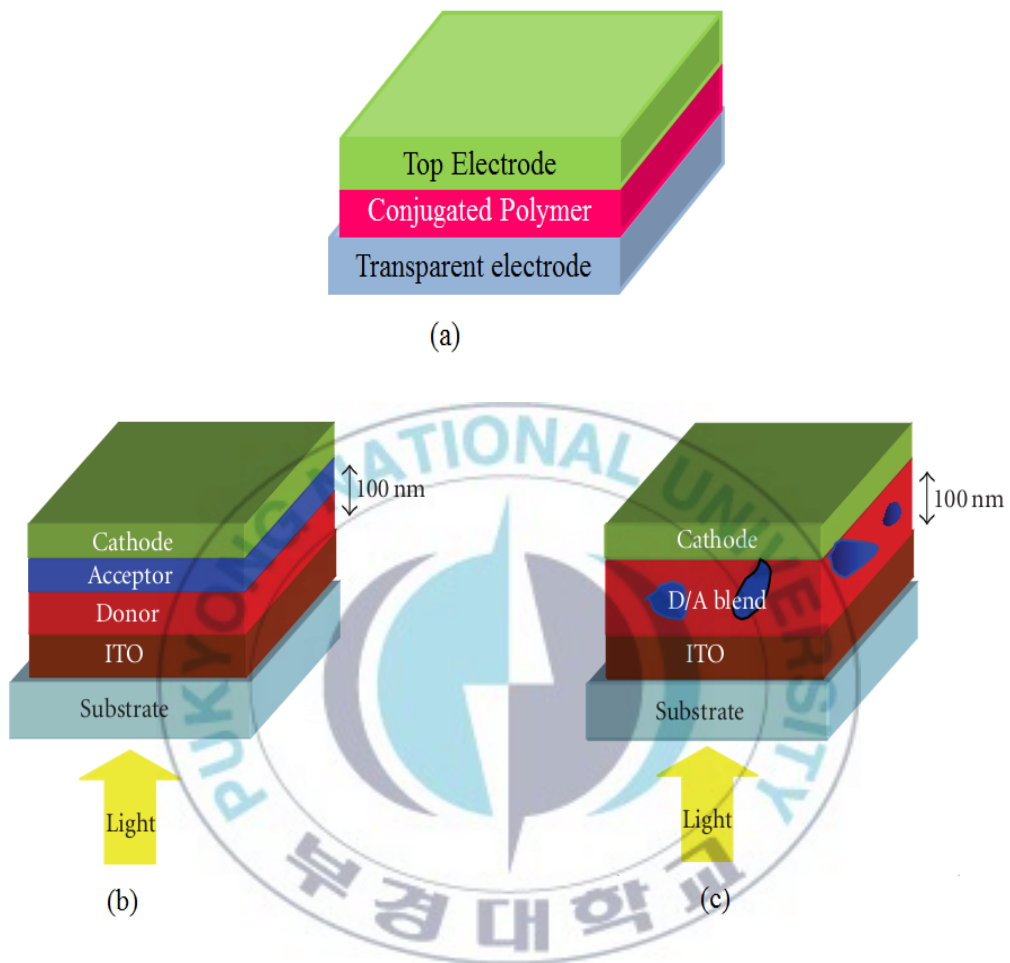


Figure I-2. The structures of OSCs:

(a) Single layer; (b) Bilayer heterojunction; (c) Bulk heterojunction

I-3. Donor and acceptor materials for OSCs

I-3-1. Donor (p-type material)

The rather short history of BHJ solar cells can be roughly divided into three phases from the perspective of the conjugated backbones of DONOR polymers. Phase one centered on poly(phenylenevinylene)s (PPV), such as poly[2-methoxy-5-(2'-ethylhexyloxy)-1,4-phenylenevinylene] (MEH-PPV) and poly[2-methoxy-5-(3',7'-dimethyloctyloxy)-1,4-phenylenevinylene] (MDMO-PPV). However, the large band gap of these polymers limited the short-circuit current density (J_{sc}). Therefore, in phase two, a smaller band gap polymer, regioregular P3HT (rr-P3HT), was thoroughly investigated. P3HT-based BHJ devices provide a noticeably higher current density (over 10 mA/cm²), attributed to its lower band gap (1.9 eV) as well as to its increased π -stacking and crystallinity which yields a higher hole mobility. Unfortunately, the high HOMO (-5.1 eV) energy level of P3HT has restricted the open-circuit voltage (V_{oc}) which consequently limits the overall efficiency. Presently in phase three, numerous polymer backbones have been reported. High V_{oc} over 1 V, high J_{sc} over 17.3 mA/cm², and fill factor (FF) over 70% have been demonstrated in different polymer-based BHJ solar cells.^[7]

I-3-2. Acceptor (n-type material)

For organic donor/acceptor based solar cells, fullerenes C60 and fullerene derivatives are the most promising acceptor materials used for organic photovoltaic applications due to its strong acceptor properties. C60 can accept according to the cyclic voltammetry investigations, up to 6 electrons. The efficient photo response of organic cells based on conjugated polymers/fullerene is due to a very fast charge transfer from the donor molecule to the acceptor. This process is faster than other recombination mechanisms, that why the quantum efficiency of this process is expected to be close to unity. The role of C60 in an organic solar cell is not only to take electrons from the polymer (donor) and to separate the exciton, but also to contribute to the conversion of the short wavelength components of sunlight. One of the disadvantages introduced by the C60 molecules is its low solubility and miscibility. This is the reason why the soluble fullerene derivative [6,6]-phenyl-C61 butyric acid methyl ester (PC₆₁BM) has become almost a standard C60 substitute material for a number of researchers working on solution processed based organic devices. In recent years, PC₇₁BM, a C70 analogue of PC₆₁BM, was used in some research groups to increase PCE because of its better light absorption in the visible region.^[1,5,6]

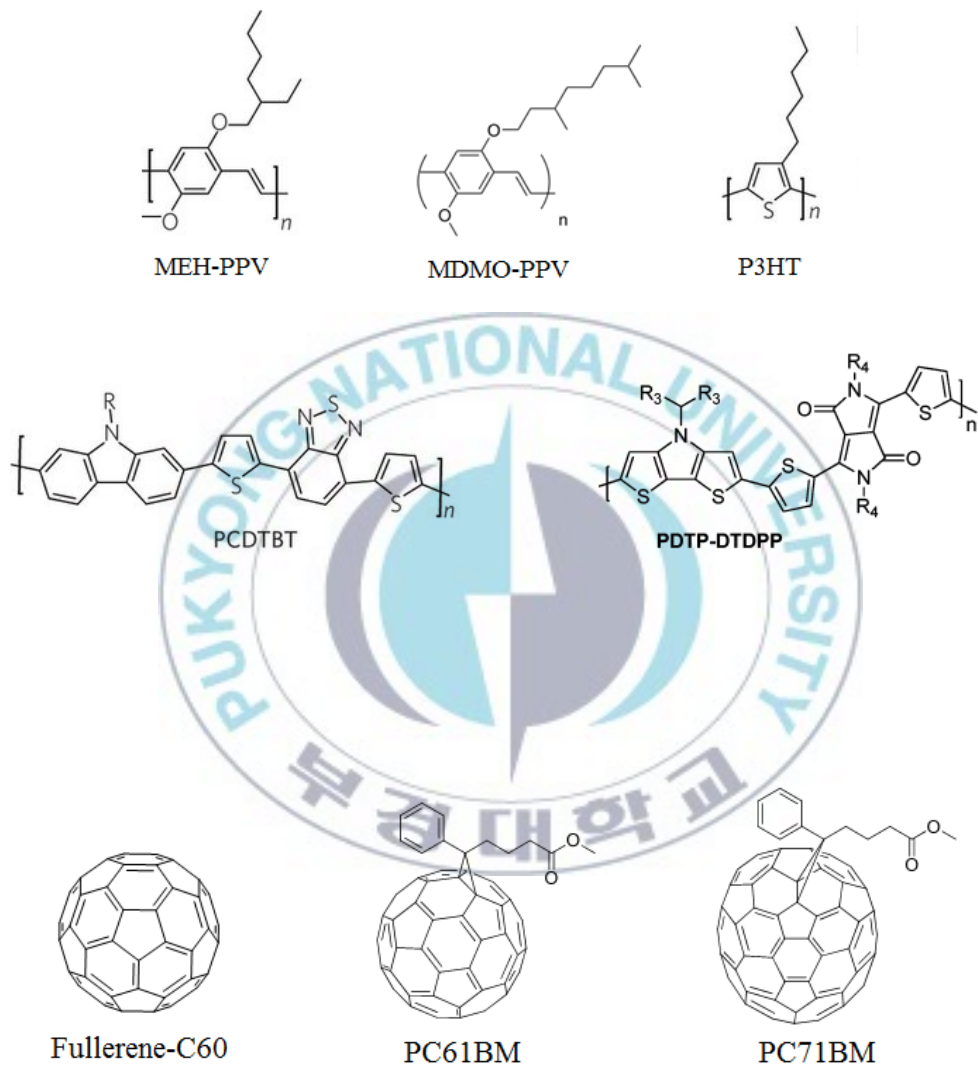


Figure I-3. Donor and acceptor materials for OSCs.

I-4. Solar cell parameters

The directly measurable parameters of a solar cell are the short-circuit current (J_{sc}), the open circuit voltage (V_{oc}), the fill factor (FF), the power conversion efficiency (PCE, η_p), and the incident photon to current efficiency (IPCE). In Figure I-5 typical J - V curves with and without illumination are shown. The dark curve shows a typical diode characteristic. Under illumination the J - V curve is shifted towards negative currents because of the photo-generated current.^[1,5,8,9]

I-4-1. Open circuit voltage (V_{oc})

The voltage at which no current flows through a solar cell is called open circuit voltage V_{oc} . Several studies have demonstrated a strong dependence of V_{oc} on the energy difference ΔE between the HOMO-LUMO (lowest unoccupied molecular orbital) offset at the DA-interface of an OSC. However, the experimental values for V_{oc} can differ from those inferred from ΔE for some material systems. This disparity can be the result of special electronic properties of the donor and acceptor at the DA-interface. Thus, a thorough understanding of molecular material properties that influence V_{oc} is important to develop new OSC materials that lead to a high V_{oc} .

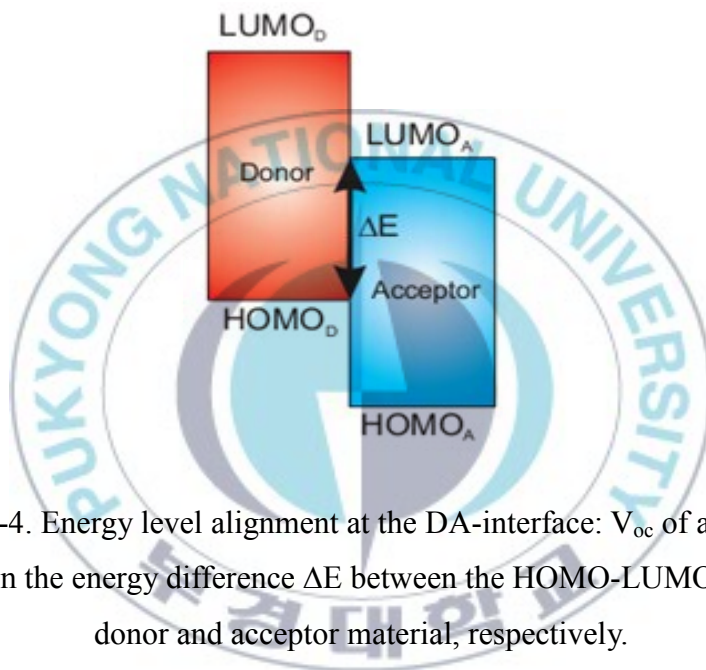


Figure I-4. Energy level alignment at the DA-interface: V_{oc} of an OSC is dependent on the energy difference ΔE between the HOMO-LUMO offset of the donor and acceptor material, respectively.

I-4-2. Short-circuit current (J_{sc})

For $V = 0$ only J_{sc} flows through the solar cell which is purely based on photo generated charge carriers. Thus, for monochromatic exposure the spectral dependence of the charge carrier generation can be measured.

I-4-3. Fill factor (FF)

The maximum electric power P_{max} of a solar cell is determined by the maximum power point in the J - V curve. Therefore, the FF is defined as:

$$FF = \frac{P_{max}}{J_{sc}V_{oc}}$$

Thus, FF is given by the ratio of gray and red areas in Figure I-5. FF is an indicator of the quality of a solar cell. The FF is significantly determined by the serial electrical resistance of the cell and therefore by the mobility of charge carriers in the organic layers of the cell. Typical values for FF are 0.75 to 0.85 in inorganic solar cells and 0.55 to 0.7 for good OSCs.

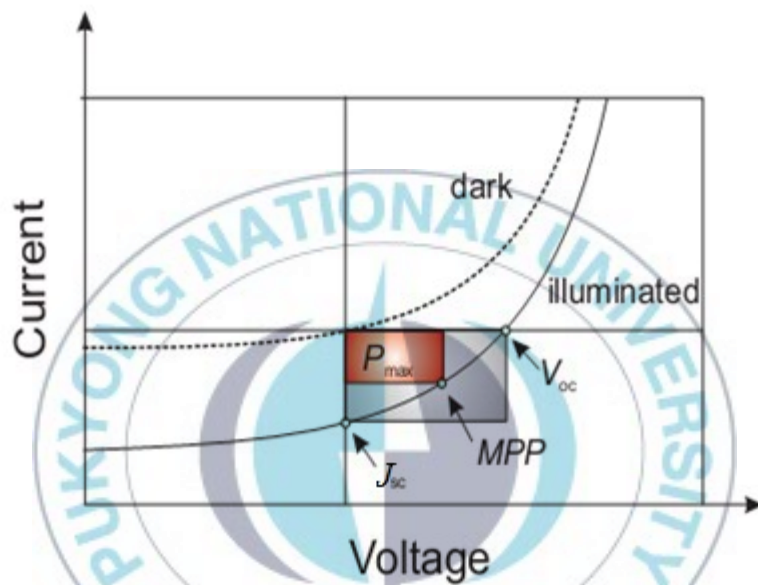


Figure I-5. J - V curves with and without illumination of a typical solar cell device. MPP is the maximum power point and P_{max} is the maximum power output of the solar cell.

I-4-4. Incident photon to current efficiency (IPCE)

The incident photon to current efficiency is defined as the ratio of the number of incident photons N_{photon} and the number of photo induced charge carriers N_{charge} which can be extracted out of the solar cell. It is smaller than the internal quantum efficiency which represents the conversion of absorbed photons into charge carriers with in the cell. The reason for this is that the IPCE takes into account the losses by reflection, scattering and recombination. In contrast to the internal quantum efficiency, which can achieve values up to almost 100%, the external quantum yield can be directly determined from the short circuit current J_{sc} and the incident light intensity J_0 :

$$\text{IPCE} = \frac{N_{\text{charge}}}{N_{\text{photon}}} = \frac{J_{\text{sc}}}{J_0} \cdot \frac{hc}{\lambda q}$$

Where q is the single electron charge, c is the speed of light, λ is the wavelength of the incident light and h is the Planck constant.

I-4-5. Power conversion efficiency (PCE, η_p)

The efficiency η_p is the maximum electrical power P_{max} per light input P_L

$$\eta_p = \frac{P_{\text{max}}}{P_L} = \frac{J_{\text{sc}} V_{\text{oc}}}{J_0} FF$$

For an efficient device a large fill factor, a large short circuit current and a large

open circuit voltage is needed. It is not sufficient to optimize only one of these parameters for efficient solar cells. Since the electrical response of the solar cell on the incident light is strongly dependent on its spectrum, standardized solar simulators which simulate an AM 1.5G spectrum are used for device characterizations.

I-5. Factors affect the efficiency of OSCs

Besides the band gap and energy level alignment another factor which is of great importance when it comes to the photovoltaic responses of OSCs is morphology. The morphology of the active layer in the device is affected by several factors: the solvent used for spin coating, concentration of the polymer, active layer thickness, composition of polymer and fullerene, annealing temperature, molecular weight and processing additives.

I-5-1. Solvent, concentration and active layer thickness

The choice of solvent was important for mixing of polymer and fullerene, for domain size and for charge transport (i.e. the solvent improved the nano-morphology).^[10] The effect of solvent on solar cell devices based on low band gap polymer is limited, however, a copolymer based on fluorine, thiophene and

benzothiadiazole with a band gap of about 2 eV showed that the morphology was improved when chlorobenzene (CB) was added to chloroform (CF) compared to spin coating from neat CF. A significant increase in J_{sc} and FF was seen, when spin coating from mixture of CF and other solvents such as CB compared to spin coating from neat CF. At the same time V_{oc} was not influenced.^[11]

The influence of solvent and concentration on device morphology and efficiency has also been investigated for polymer based on benzodithiazone and thiophene derivative in BHJ devices. The efficiency was shown to depend on the solvent, the spin rate, the spin time and the concentration. For this polymer a higher efficiency was achieved when the active layer was spin coated from 1,2-dichlorobenzene (DCB) compared to spin coating from a mixture of CF and CB.

Spin coating time and spin rate was found to produce thin films when using high rates and short times (slow dried film) and thick films when using low rates and long time (fast dried film). An improved efficiency was achieved for the slowly dried film. Concentration of this polymer with a fixed ratio (1:2) of PCBM and the same solvent (DCB) showed that the efficiency increased with an increase in concentration and film thickness from 0.42% for a 35 nm thick film to 0.9% for a 120 nm thick film. However, increasing the concentration of the polymer further and hence, the film thickness, resulted in a decrease in the efficiency to 0.39% for a 270 nm thick film.

I-5-2. Ratio between polymer and fullerene

The ratio between the polymer and the fullerene in BHJ devices is of great importance in terms of photovoltaic response. The optimum ratio depends on the type of polymer mixed with PCBM. For MEHPPV the ratio which gave the highest efficiency was 1:3 and 1:4. This was not the case for P3HT or a copolymer of benzothiadiazole, thiophene and pyrrole, where ratios of 1:1 between the polymer and PCBM have been shown to be optimum. The morphology is affected by the ratio between the polymer and PCBM. Addition of more PCBM to P3HT has been shown to increase electron mobility.^[12,13]

I-5-3. Annealing temperature

Several groups have reported on the annealing of OSC devices based on P3HT and PCBM. Both post-production annealing and pre-treatment annealing (i.e. annealing before and after deposition of the aluminum electrode) have been carried out. This showed that the pretreatment resulted in a rougher surface which causes an increase in the efficiency of the device due to larger contact area between the polymer and the electrode. The post annealing also resulted in improved efficiency but the cause of this is not known. Annealing of a device has been shown to increase the charge carrier separation efficiency and the mobility

of the charge carriers due to phase segregation. It has been shown that upon annealing of a BHJ based on P3HT and PCBM, the PCBM diffuses out of the polymer matrix and the polymer then orders in the lamella structure. The PCBM clusters improve the photocurrent due to formation of percolation paths.^[14]

I-5-4. Molecular weight

The molecular weight has been shown to influence the carrier mobility, the morphology and consequently, the efficiency of OSC devices. Results obtained for copolymers of dithienosilole and thienopyrrolodione (PDTSTPDs) show that high molecular weight results in higher efficiencies due to higher carrier mobility and better film morphology. When the molecular weight increased from 10 kDa to 18 kDa and 31 kDa, the hole mobility of the PDTSTPD-C8 increased from 7×10^{-6} to 1×10^{-4} and $3.7 \times 10^{-4} \text{ cm}^2 \text{ V}^{-1} \text{ s}^{-1}$. Besides, its solubility decreased and it tended to form aggregates. As a result, the domain size became larger ($\approx 20 \text{ nm}$ in width, still comparable to the exciton diffusion length) and, meanwhile, less discontinuous phase separation was observed. Therefore PCE of devices were improved from 3.1 to 3.4 and 7.7%.^[15]

I-5-5. Processing additives

Recently, to improve morphology of active layer, OSC processing additives offer an attraction over annealing processes in that they do not require an additional fabrication step. Two general guidelines for additive design are follows: (1) the boiling point must be significantly greater than that of the processing solvent to maximize the interaction time between the additive and the active layer components during thin film formation and (2) one active layer component must be significantly more soluble in the additive than the other components.

2.5% of 1,8-diiodooctane (DIO) was added to active solution comprising dithiophene-benzothiadiazole (PCPDTBT) and PC₇₁BM. Because the DIO has a higher boiling point than the CB host solvent, the PCBM tends to remain in solution (during drying) longer than the semiconducting polymer, thereby enabling control of the phase separation and the resulting morphology of the BHJ material. DIO selectively dissolves PC₇₁BM aggregates, allowing their intercalation into PCPDTBT domains, thereby optimizing both the domain size and the PCPDTBT-PC₇₁BM interface. Therefore the performances of solar cells based on PCPDTBT/ PC₇₁BM processed with DIO as the processing additive are higher than those of devices without using the processing additive. PCE increased from 3.4 to 5.1%.^[16, 17]

I-5-6. Other factors

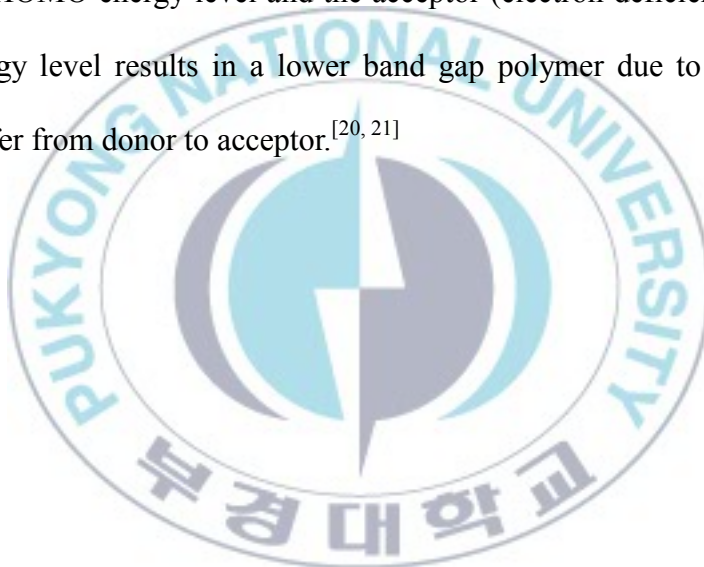
Besides these factors, other studies have shown that the morphology of the active layer is also affected by the size of the active area. Generally, the efficiency often decreases with an increase in the active area due to poorer morphology in the larger active area device. The type of compound also affects the photovoltaic response of OSC devices.^[18] The low band gap polymers are believed to increase the efficiency of the device compared to other types of polymers applied in OSCs. The morphology has also been shown to depend on the types of side chains on the polymer backbone and on the position of the side chains. In a copolymer of thienopyrazine and thiophene a higher efficiency was achieved for the polymer with bulky side groups on the benzene ring compared with bulky side groups on the thiophene ring.^[19] Studies have shown that a low band gap alone is not enough to ensure a high efficiency. The way that the molecules order in the solid phase is of great importance as for example in the case of P3HT which orders in a lamellar structure.

I-6. Low Band gap Polymers

For conjugated polymers used in OSC devices, band gap (E_g) and molecular energy levels are of crucial importance for device performance. The mismatch between absorption spectra of conjugated polymers and the solar irradiance spectrum is one of the main reasons for low efficiency of OSC devices. Therefore, in the design and synthesis of high efficiency polymer photovoltaic materials, low band gap conjugated polymers have been broadly pursued in recent years. The spectrum of photon flux of sunlight exhibits a broadband in the range from 350 to 3000 nm with a peak at about 680 nm. To make the absorption spectra of the conjugated polymers match the solar spectrum, their absorption maximum should be at ca. 700 nm, which means that the band gap of the conjugated polymers should be lower than 1.74 eV.^[20, 21] In fact, over the last decade, rr-P3HT was intensively investigated for its high carrier mobility, and through the morphology control of P3HT/[6,6]phenyl-C61-butyric acid methyl ester (PC₆₁BM), PCE approached near 5%. Despite P3HT/PCBM show good performance, the large band gap of P3HT (1.9 eV) is not ideal material for polymer solar cell to improve the solar spectrum harvest because the absorption spectrum of P3HT only covers the range of 300-650 nm. In order to improve light harvesting by OSCs, two approaches are the most widely adopted to reduce the band gap of conjugated polymers.^[22] One is to increase the quinoid character of the polymer neutral state,

such as in polythieno[3,4-b]thiophene, in which the thiophene ring is fused with another thiophene unit. The other is the introduction of strong push-pull intramolecular interactions into the polymer backbone, such as in the most common donor–acceptor polymers (D-alt-A polymers).^[23]

The most successful approach to achieving low band gap polymers is a copolymerized D–A structure. The copolymerization of the donor (electron-rich) with higher HOMO energy level and the acceptor (electron deficient) with lower LUMO energy level results in a lower band gap polymer due to an intrachain charge transfer from donor to acceptor.^[20, 21]



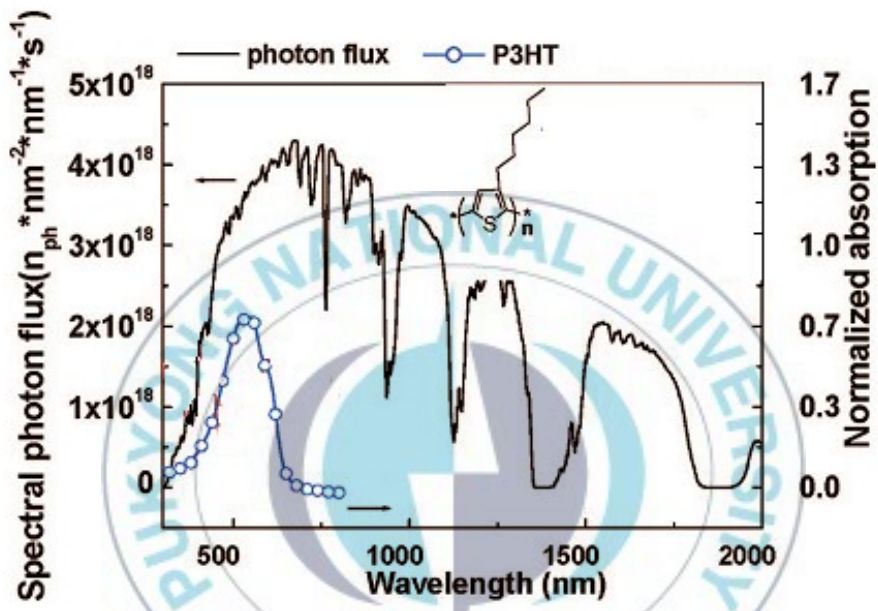


Figure I-6. Solar photon flux (the solid line) spectrum (AM 1.5G) and absorption spectrum of P3HT (the line with circles).

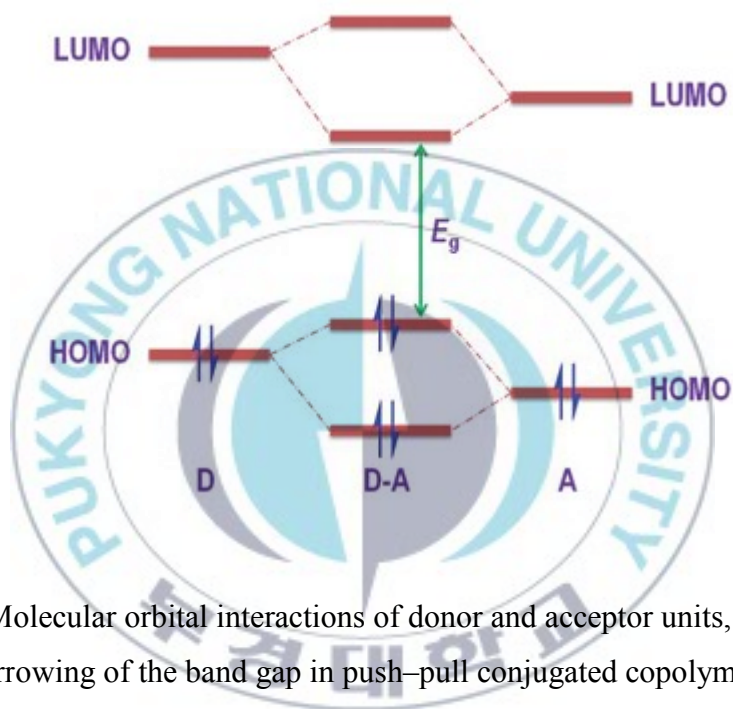


Figure I-7. Molecular orbital interactions of donor and acceptor units, resulting in a narrowing of the band gap in push-pull conjugated copolymers.

Chapter II. Synthesis and Characterization of π -Conjugated Polymers Based on 2-Arylbenzimidazole and 4,7-Di-2-thienyl-2,1,3-benzothiadiazole

II-1. Introduction

According to the reports of Yamamoto et al. on n-type π -conjugated units, benzimidazole, benzothiadiazole, benzotriazole and benzoselenadiazole are potentially acceptor units and their electrochemical and optical characteristics are slightly different since they possess different atoms on their isoelectronic structures.^[24] Among them, benzimidazole has been little studied. However, the preparation of homologues of benzimidazole and revealing their chemical and physical properties has also been paid too much attention recent years.

Benzimidazole is an interesting building block for π -conjugated polymers, because it shows interesting chemical properties such as photoluminescence, solvatochromism, and metal-complex forming reactivity. Besides, it also exhibits high electron transporting ability because of the electron withdrawing imine (C=N) bonds on their backbones similar to pyridine and quinoxaline.^[24, 25]

In this work, we take advantage of structural feature of benzimidazole to synthesize new conjugated copolymers. 2-Arylbenzimidazole derivative was

incorporated with 4,7-di-2-thienyl-2,1,3-benzothiadiazole as electron poor units, 9,9-dioctylfluorene as electron rich unit and thiophene as the bridge based copolymer through Suzuki coupling reaction. These copolymers can be promisingly applied to fabricate OSC devices or polymer light-emitting device...

II-2. Experimental Section

II-2-1. Materials and Synthesis

Methylene chloride (MC) was distilled over calcium hydride (CaH_2). All other chemicals were purchased from Sigma-Aldrich Co, Tokyo Chemical Industry (TCI) or Alfa Aesar (A Johnson Matthey Company) and used as received unless otherwise described.

II-2-1-1. 3,6-Dibromo-benzene-1,2-diamine (1)^[26]

To a suspension of 4,7-dibromo-2,1,3-benzothiadiazole (4.41 g, 15 mmol) in ethanol (150 mL) was added slowly sodium borohydride (NaBH_4 , 6.81 g, 0.18 mol) at 0 °C, and the mixture was stirred for 12 hours at room temperature. After evaporation of the solvent, 200 mL of water was added, and the mixture was extracted with diethylether. The extract was dried over anhydrous magnesium

sulfate (MgSO₄), evaporated the solvent and then recrystallized by hexane; a white solid compound was obtained (2.99 g, 75%). ¹H-NMR (400 MHz, CDCl₃, ppm): δ 6.82 (s, 2H), 3.88 (s, 4H).

II-2-1-2. 4,7-Dibromo-2-(4-*tert*-butyl-phenyl)-1*H*-benzoimidazole (2)^[27]

4-*Tert*-butyl-benzaldehyde (1.8 mL, 10.5 mmol) was added dropwise to a mixture of 3,6-dibromo-benzene-1,2-diamine (2.66 g, 10 mmol) and sodium hydrogen sulfite (NaHSO₃, 1.04 g, 10 mmol) in dimethylacetamide (DMA, 10 mL) at 100 °C. The mixture was refluxed at 100 °C for 4 hours on an oil bath. After cooling the mixture to room temperature, a portion of 100 mL of water was added and the mixture was extracted with ethyl acetate (EA). The combined organic phase was dried over anhydrous MgSO₄ and concentrated under reduced pressure. The crude product was purified through column chromatography using hexane:EA (4:1, v/v) to provide 4,7-dibromo-2-(4-*tert*-butyl-phenyl)-1*H*-benzoimidazole as a white solid (3.31 g, 81%). ¹H-NMR (400 MHz, DMSO-*d*₆, ppm): δ 9.3 (s, 1H), 8.27~8.25 (d, *J* = 8.4 Hz, 2H), 7.60~7.58 (d, *J* = 8.4 Hz, 2H), 3.37 (s, 2H), 1.34 (s, 9H).

**II-2-1-3. 4,7-Dibromo-2-(4-*tert*-butyl-phenyl)-1-ethyl-1*H*-benzoimidazole
(3)^[28]**

4,7-Dibromo-2-(4-*tert*-butyl-phenyl)-1*H*-benzoimidazole (3.27 g, 8 mmol) was dissolved in 20 mL of dimethyl formamide (DMF) and stirred vigorously with potassium carbonate (K₂CO₃, 3.32 g, 24 mmol) at room temperature for an hour. The mixture of ethyl iodine (C₂H₅I, 1.29 mL, 16 mmol) in 10 mL of DMF was added dropwise with dropping funnel at 50 °C and then the mixture was stirred for 6 hours. After cooling the mixture to room temperature, 100 mL of water was added and the mixture was extracted with EA. The organic phase was collected and dried by anhydrous MgSO₄. Removal of the solvent and column purification on silica gel using hexane and EA mixed eluent (10:1, v/v) yielded 4,7-dibromo-2-(4-*tert*-butyl-phenyl)-1-ethyl-1*H*-benzoimidazole as a white solid (3.0 g, 86%).
¹H-NMR (400 MHz, CDCl₃, ppm): δ 7.59~7.57 (d, *J* = 8.4 Hz, 2H), 7.52~7.49 (d, *J* = 8.4 Hz, 2H), 7.32~7.30 (d, *J* = 8.4 Hz, 1H), 7.28~7.26 (d, *J* = 8.4 Hz, 1H), 4.56~4.50 (m, 2H), 1.38~1.34 (m, 12H).

II-2-1-4. 2-(4-*Tert*-butyl-phenyl)-1-ethyl-4,7-di-thiophen-2-yl-1*H*-benzoimidazole (4)^[29]

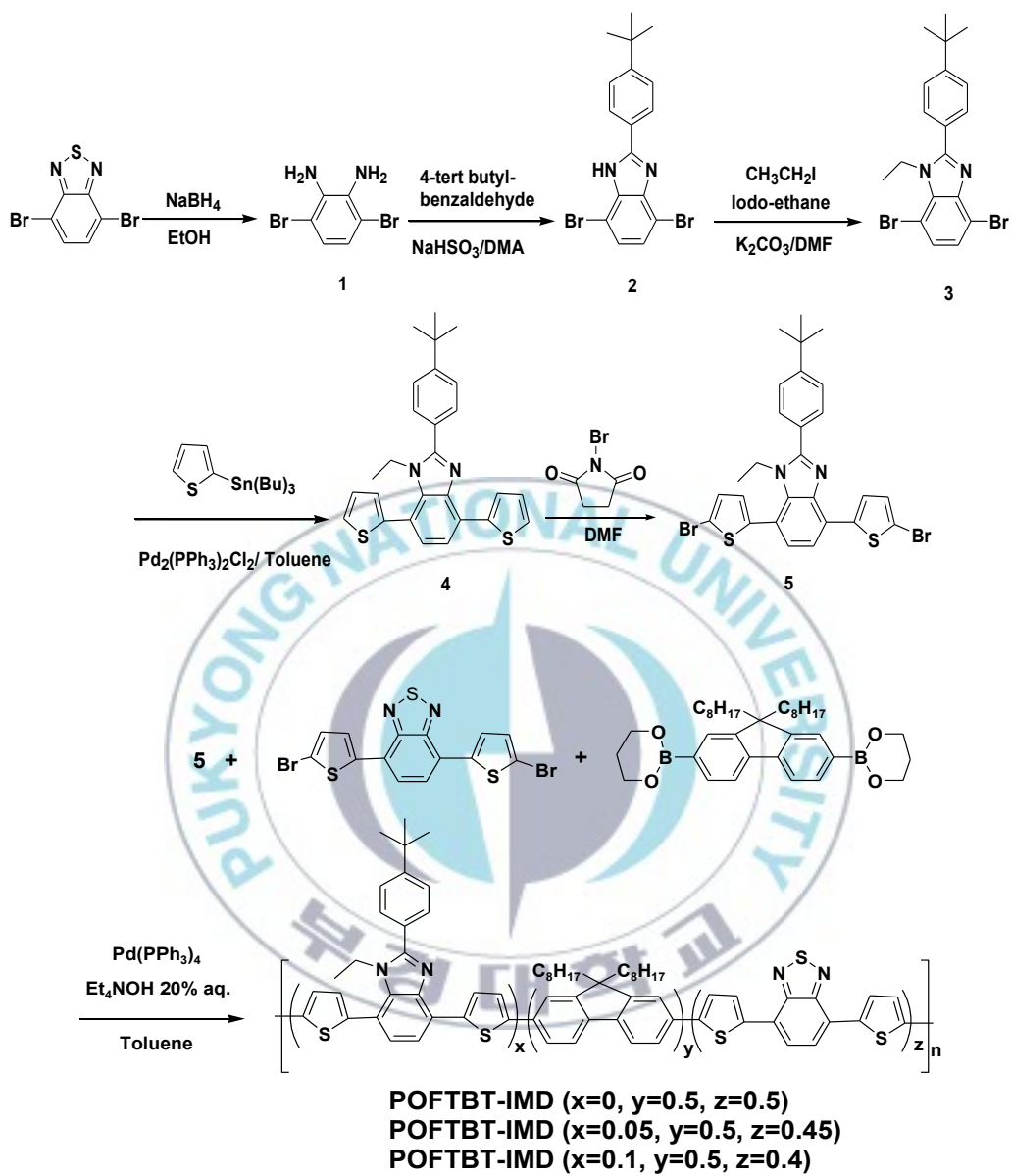
To a solution of 4,7-dibromo-2-(4-*tert*-butyl-phenyl)-1-ethyl-1*H*-benzoimidazole (2.97 g, 6.8 mmol) and tributyl(2-thienyl)stannane (5.6 g, 15 mmol) in toluene (50 mL), bis(triphenylphosphine)palladium(II) dichloride (PdCl₂(PPh₃)₂, 0.28 g, 5 mol%) was added. The mixture was refluxed under a nitrogen atmosphere for 12 hours. After cooling the mixture to room temperature, a portion of 100 mL of water was added and the mixture was extracted with EA. The organic extraction was dried with anhydrous MgSO₄ and the solvent was removed by vacuum evaporation. The residue was purified by column chromatography with hexane:MC (1:1, v/v) as eluent, yielding 2-(4-*tert*-butyl-phenyl)-1-ethyl-4,7-di-thiophen-2-yl-1*H*-benzoimidazole as a yellow solid (2.11 g, 70%). ¹H-NMR (400 MHz, CDCl₃, ppm): δ 8.20~8.19 (dd, *J*₁ = 1.2 Hz, *J*₂ = 3.6 Hz, 1H), 7.69~7.67 (d, *J* = 8.3 Hz, 2H), 7.60~7.58 (d, 7.9 Hz, 1H), 7.53~7.51 (d, *J* = 8.6 Hz, 2H), 7.42~7.41 (dd, *J*₁ = 1.2 Hz, *J*₂ = 5.2 Hz, 1H), 7.36~7.34 (dd, *J*₁ = 1.2 Hz, *J*₂ = 5.2 Hz, 1H), 7.26~7.25 (d, *J* = 2.8 Hz, 1H), 7.16~7.12 (m, 3H), 4.16~4.10 (m, 2H), 1.37 (s, 9H), 0.86~0.83 (t, *J* = 7.0 Hz, 3H).

II-2-1-5. 4,7-Bis-(5-bromo-thiophen-2-yl)-2-(4-*tert*-butyl-phenyl)-1-ethyl-1*H*-benzoimidazole (5)

2-(4-*Tert*-butyl-phenyl)-1-ethyl-4,7-di-thiophen-2-yl-1*H*-benzoimidazole (0.89 g, 2 mmol) was dissolved in DMF under nitrogen atmosphere, and the *N*-bromosuccinimide (NBS; 1.07 g, 6 mmol) was added in one portion. The reaction mixture was stirred overnight at room temperature and then the mixture was quenched with 50 mL of water and extracted with EA. The combined organic extract was with aqueous NaHSO₃ (10 wt.%) and concentrated under reduced pressure to afford a crude product that was purified to column chromatography using hexane:MC (4:1, v/v) to get 4,7-bis-(5-bromo-thiophen-2-yl)-2-(4-*tert*-butyl-phenyl)-1-ethyl-1*H*-benzoimidazole as a white solid (0.6g, 50%). ¹H-NMR (400 MHz, CDCl₃, ppm): δ 7.73~7.71 (d, *J* = 7.7 Hz, 1H), 7.62~7.59 (m, 2H), 7.51~7.49 (m, 2H), 7.26~7.24 (d, *J* = 7.32 Hz, 2H), 7.09~7.05 (m, 2H), 6.93~6.92 (d, *J* = 3.7 Hz, 1H), 4.18~4.13 (m, 2H), 1.34 (s, 9H), 0.93~0.90 (t, *J* = 7.0 Hz, 3H).

II-2-1-6. Synthesis of Polymers POFTBT-IMD

9,9-Dioctylfluorene-2,7-diboronic acid bis(1,3-propanediol) ester (0.1117 g, 0.2mmol), 4,7-bis(5-bromo-2-thienyl)-2,1,3-benzothiadiazole (TBT, 0.0623 g/0.136 mmol for IMD10 and 0.0701 g/ 0.153 mmol for IMD5), compound 5 (0.0204 g/0.034 mmol for IMD10 and 0.0102 g/0.017 mmol for IMD5) and tetrakis(triphenylphosphine)palladium(0) ($\text{Pd}(\text{PPh}_3)_4$, 0.0115 g, 0.01 mmol) were dissolved in 3 mL of toluene and purged under a nitrogen atmosphere for 10 min. Subsequently, tetraethylammonium hydroxide 20% in water (0.8 mL) was added into a flask. The reaction mixture was stirred at 65 °C for 2 hours. Bromobenzene was added and stirred for 1 hour. After being cooled to room temperature, the reaction mixture was poured into methanol. The solid was filtered and re-dissolved in chloroform. Ammonium hydroxide solution was added and stirred overnight. The organic layer was washed with deionized water twice. Then it was precipitated in a large amount of methanol. The solid was filtered and further purified by Soxhlet extractor using methanol and then hexane for 12 hours. Solid was filtered and dried in vacuum. A dark red powder POFTBT-IMD was obtained, and the yield was 70%.



Scheme II-1. Synthesis of monomer and polymer (POFTBT-IMD).

II-2-2. Measurement

Synthesized compounds were characterized by $^1\text{H-NMR}$ spectrum, which were obtained with a JEOL JNM ECP-400 spectrometer. The thermogravimetric analysis (TGA) was carried out under the N_2 atmosphere at a heating rate of $10\text{ }^\circ\text{C}/\text{min}$ with a Perkin-Elmer TGA 7 thermal analyzer. UV-Vis and photoluminescence (PL) spectra of the polymers were recorded using a JASCO V-530 Spectrophotometer and a HITACHI F-4500, respectively. The cyclic voltammetry (CV) was performed by an Ivium B14406 with a three electrode cell in a solution of Bu_4NPF_6 (0.1 M) in freshly distilled MC at a scan rate of 100 mV/s . Pt wires were used as the counter and working electrode and a Ag/Ag^+ electrode was used as the reference electrode.

II-3. Results and Discussion

II-3-1. Thermal Properties

All the polymers exhibited good thermal stability with 5% weight-loss temperatures (T_d) higher than 285 °C under N_2 , as revealed by thermogravimetric analysis (TGA) (see Figure II-1). T_d values of POTBT, POFTBT-IMD5 and POFTBT-IMD10 were 376, 436 and 285 °C, respectively. The thermal stability of the polymers is favorable for its application in OSCs and other optoelectronic devices.



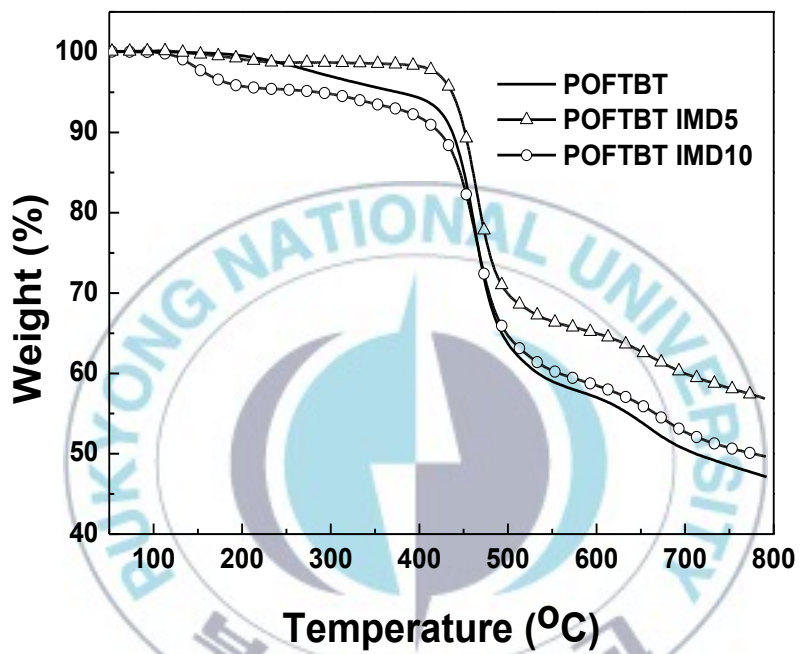


Figure II-1. TGA thermogram of polymers POTBT, POFTBT-IMD5 and POFTBT-IMD10 with a heating rate of $10\text{ }^{\circ}\text{C min}^{-1}$ under a N_2 atmosphere.

II-3-2. Optical Properties

The photo-physical characteristics of the polymers were investigated by UV-Vis absorption spectrometer. Figure II-2 showed the absorption spectrum of POFTBT, POFTBT-IMD5 and POFTBT-IMD10. All of the polymers had absorption around 360-420 nm which we assign to localized π - π^* transition bands, and the other broad absorption signals around 540~580 nm which were attributed to internal charge transfer (ICT) interactions between the TBT, IMD acceptor moieties and 9,9-dioctylfluorene donor units. The maximum UV-Vis absorption peaks (λ_{\max}) of three polymers located at 558, 559, 555 nm and optical band gaps (E_g^{opt}) estimated from the absorption edge (λ_{edge}) in the UV-Vis spectrum of the thin solid film by formula $E_g^{\text{opt}} = 1240/\lambda_{\text{edge}}$. The E_g^{opt} values of POFTBT, POFTBT-IMD5 and POFTBT-IMD10 were 1.93, 1.93 and 1.94, respectively.

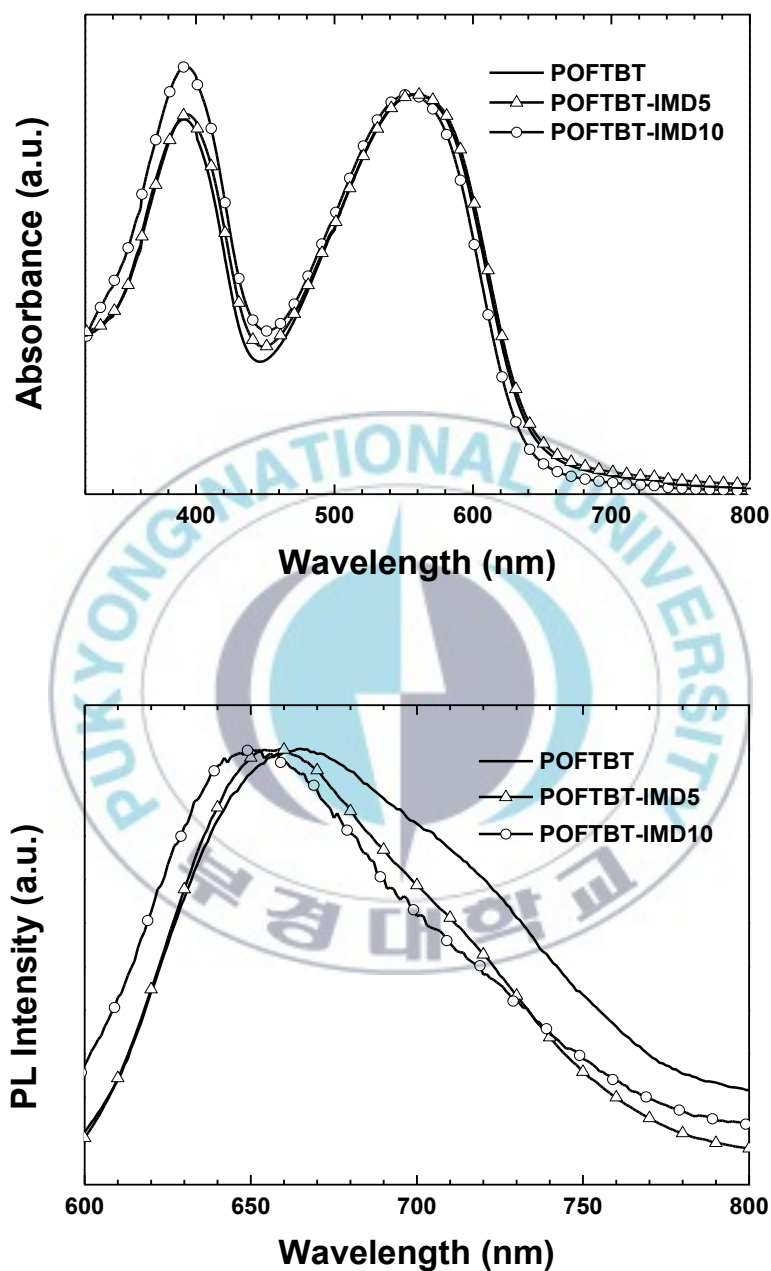


Figure II-2. Normalized UV-Vis absorption and Photoluminescence spectrum of POFTBT, POFTBT-IMD5 and POFTBT-IMD10.

II-3-3. Electrochemical Properties

The information about energy levels of π -conjugated polymer is very important to determine V_{oc} and the charge separation of OSCs. Cyclic voltammetry was used to estimate the HOMO and LUMO energy levels of polymers. Polymers underwent quasi-reversible p-doping and irreversible n-doping process in the positive and negative scans. The energy levels of polymers were calculated from the onset potential of oxidation by assuming the energy level of ferrocene (Fc) as -4.8 eV.

The LUMO energy levels of POFTBT, POFTBT-IMD5 and POFTBT-IMD10 figured out from the reduction onset potential were -3.7, -3.84, -3.81 eV, respectively. The HOMO energy levels of POFTBT, POFTBT-IMD5 and POFTBT-IMD10 were -5.3, -5.4, -5.4 eV, respectively. The optical and electrochemical properties of polymers were summarized in Table II-1.

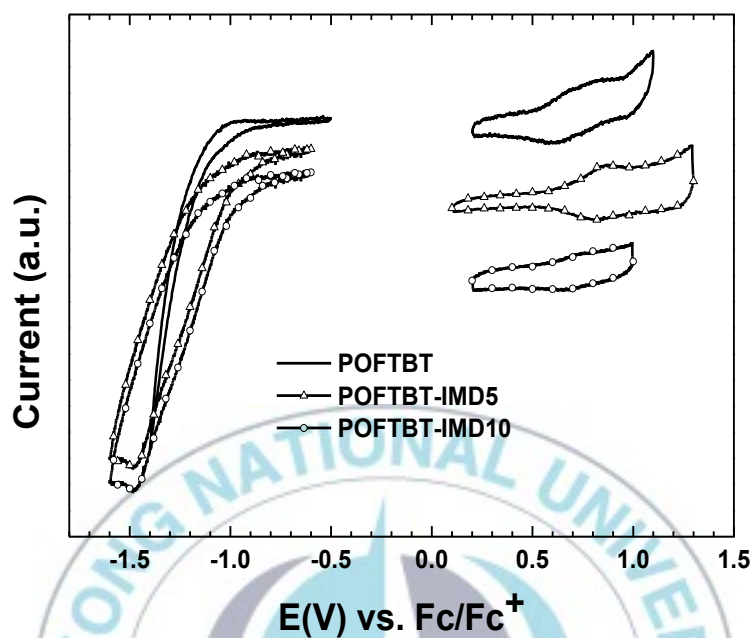


Figure II-3. Cyclic voltammogram of POFTBT, POFTBT-IMD5 and POFTBT-IMD10.

Table II-1. Optical absorption and electrochemical properties of POFTBT, POFTBT IMD5 and POFTBT IMD10.

Polymer	λ_{\max} (nm)	PL_{\max} (nm)	E_g^{opt} (eV) ^a	HOMO (eV) ^b	LUMO (eV) ^c
POFTBT	558	665	1.93	-5.3	-3.7
POFTBT-IMD5	559	653	1.93	-5.4	-3.84
POFTBT-IMD10	555	659	1.94	-5.4	-3.81

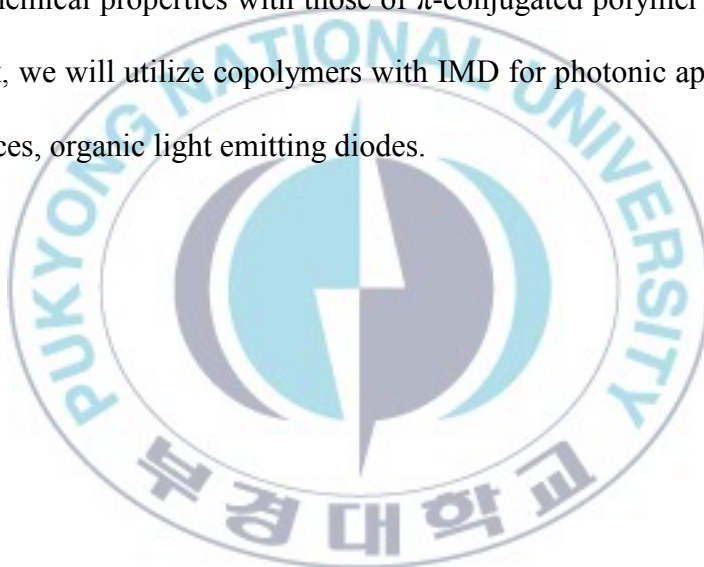
^a Estimated from the absorption edge of UV-Vis spectrum

^b Figured out from the oxidation onset potential

^c Figured out from the reduction onset potential

II-4. Conclusions

We synthesized copolymers with 9,9-dialkylfluorene, 4,7-di-2-thienyl-2,1,3-benzothiadiazole (TBT) and 2-(4-*tert*-butyl-phenyl)-1-ethyl-4,7-di-thiophen-2-yl-1*H*-benzimidazole (IMD) through the Suzuki coupling reaction. New π -conjugated copolymers POFTBT-IMD5, POFTBT-IMD10 showed similar optical and electrochemical properties with those of π -conjugated polymer without IMD. Further work, we will utilize copolymers with IMD for photonic application such as OSC devices, organic light emitting diodes.



Chapter III. Synthesis and Characterization of π -Conjugated Polymer Based on Arylene Imide for Organic Solar Cells

III-1. Introduction

From a material point of view, the alternating donor–acceptor (DA) system has been regarded as the most effective method for developing organic photovoltaic materials, since polymer band gaps could be easily controlled by inducing orbital overlap between donor and acceptor materials. However, there are a few of electron-donating and electron withdrawing candidate materials for high performance polymeric photovoltaic materials. Particularly, since electron withdrawing materials have various restrictions, such as insolubility, electron affinity, instability, etc., the number of electron withdrawing materials is smaller compared to the number of electron-donating materials in DA-type polymers for organic photovoltaic. Nevertheless, the electronic and chemical properties of electron withdrawing moieties are very important parameters for determining that of polymers in DA-type copolymers.^[30,31]

Recently, arylene imide has emerged as an attractive candidate for electron-accepting unit in the D-A copolymers due to its high electron affinity and charge transport properties.^[32] One advantage of using imides as electron-withdrawing groups is the imide nitrogen atom provides an open position for alkylation

directed away from adjacent backbone units. As we know, a challenge in organic semiconductor is to maintain a balance between solubility and close π - π stacking. Alkyl side chains can impart solubility to polymers, but their effect on backbone planarity and packing depends critically on their placement. However, imide groups provide such open positions for alkylation without sacrificing conjugation and therefore coplanarity and efficient π - π stacking can be maintained by judicious choice of donor monomers. Besides, arylene imide with 2 carbonyl bonds (C=O) is strong electron withdrawing group results in air stable and low-lying HOMO which leads to improve the V_{oc} values of final devices.^[33-35]

Figure III-1 and Table III-1 present the chemical structures, band gaps, HOMO levels, and photovoltaic properties of conjugated polymers based on arylene imides which were reported by some groups.

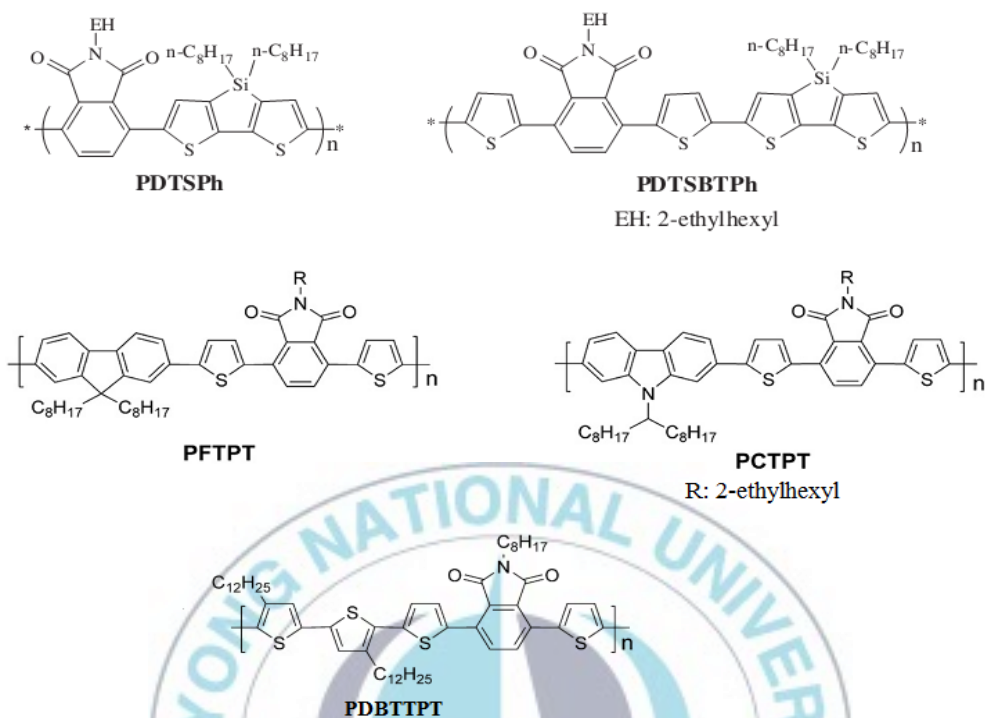


Figure III-1. Chemical structures of copolymers based on arylene imide.

Table III-1. Summary of band gaps, HOMO levels, and photovoltaic properties of conjugated polymers based on arylene imide.

Polymer	E_g^{opt} (eV)	HOMO (eV)	J_{sc} (mA/cm ²)	V_{oc} (V)	FF (%)	PCE (%)	Ref.
PDTSPh	2.03	-5.25	2.39	0.73	33	0.58	33
PDTSBTPh	1.93	-5.19	6.27	0.83	40.4	2.1	33
PFTPT	2.4	-5.62	1.90	0.90	27	0.47	34
PCTPT	2.36	-5.52	4.41	0.94	33	1.4	34
PDBTTPT	1.96	-5.34	5.9	0.81	30	1.5	35

Herein, we modify arylene imide compound by introducing two decyloxy groups to 5- and 6- position of benzene ring which is very helpful for the construction of the conjugated polymers with better solubility and high molecular weight. The good solubility of conjugated polymers is crucial for its purification and the formation of high quality film for efficient OSC devices. Whereas, the molecular weight of polymers can significantly influence the performance of OSCs, usually the high molecular weight sample gives better photovoltaic performance than the low molecular weight sample. Besides, we also add a butyl group on nitrogen atom to form the new acceptor moiety 2-butyl-5,6-bis-decyloxy-4,7-di-thiophen-2-yl-isoindole-1,3-dione. This compound was incorporated into thiophene rings through the Stille coupling reaction. The newly synthesized polymer was investigated and explored in BHJ solar cells.

III-2. Experimental Section

III-2-1. Materials and Synthesis

Methylene chloride (MC) was distilled over CaH_2 . All other chemicals were purchased from Sigma-Aldrich Co, Tokyo Chemical Industry (TCI) or Alfa Aesar (A Johnson Matthey Company) and used as received unless otherwise described.

III-2-1-1. 1,2-Bis-decyloxy-benzene (1)

Sodium hydroxide (NaOH, 8 g, 0.2 mol) was dissolved in methanol (200 mL) at 0 °C for 30 min and then catechol (10 g, 90.82 mmol) was added slowly. White solution turned to deep green and finally dark. At this time 1-bromodecane (42.5 mL, 0.2 mmol) was put into the mixture dropwise. Next, the mixture was refluxed in a dry nitrogen atmosphere with stirring. After 8 hours, reaction mixture was cooled down to room temperature and evaporated to eliminate methanol. 250 mL of water and EA were added to extract. The organic layer was separated, dried over MgSO₄ and concentrated. The combined organic layer was triturated from methanol (26.6 g, 75%). ¹H-NMR (400 MHz, CDCl₃, ppm): δ 6.87 (s, 4H), 3.99~3.95 (t, *J* = 7.0 Hz, 4H), 1.83~1.76 (m, 4H), 1.48~1.41 (m, 4H), 1.33~1.26 (m, 24H), 0.88~0.85 (t, *J* = 7.0 Hz, 6H). ¹³C-NMR (100 MHz, CDCl₃, ppm): δ 150.29, 122.34, 115.46, 65.81, 32.89, 30.24, 30.51, 30.44, 30.19, 29.65, 26.09, 23.67, 15.05.

III-2-1-2. 1,2-Diiodo-4,5-bis-decyloxy-benzene (2)^[36]

1,2-Bis-decyloxy-benzene (15.63 g, 40 mmol), iodine (I₂, 9.14 g, 36 mmol), iodic acid (HIO₃, 4.22 g, 24 mmol), and sulfonic acid (H₂SO₄, 30% aqueous solution, 12 mL) in carbon tetrachloride (CCl₄, 4 mL) and acetic acid (150 mL) were heated at 75 °C overnight under stirring. The resulting mixture was cooled, diluted with water (50 mL) and extracted with EA. The organic phase was washed with an aqueous solution of NaHSO₃ (10%, 100 mL) and water (100 mL), dried over anhydrous MgSO₄, and the solvent evaporated at reduced pressure. The crude product was purified by column chromatography with 100% hexane. 20.56 g (yield: 80%) of white solid was obtained. ¹H-NMR (400 MHz, CDCl₃, ppm): δ 7.22 (s, 2H), 3.91~3.88 (t, *J* = 6.6 Hz, 4H), 1.80~1.73 (m, 4H), 1.45~1.38 (m, 4H), 1.28~1.25 (m, 24H), 0.88~0.84 (t, *J* = 6.6 Hz, 6H). ¹³C-NMR (100 MHz, CDCl₃, ppm): δ 150.83, 124.83, 97.02, 70.54, 32.97, 30.65, 30.62, 30.4, 30.1, 30.02, 26.98, 23.74, 15.18.

III-2-1-3. 1,2-Dicyano-4,5-bis-decyloxy-benzene (3)^[37]

A suspension of 1,2-diiodo-4,5-bis-decyloxy-benzene (19.27 g, 30 mmol) and copper(I)cyanide (CuCN, 12.1 g, 135 mmol) in DMF (80 mL) was refluxed overnight under an atmosphere of dry nitrogen. The cooled reaction mixture was then poured into solution of hydrated ferric chloride (58.38 g, 216 mmol) in 90 mL of 2M hydrochloric acid and stirred vigorously for 1 hour at 60-70 °C. After filtration the mixture was extracted four times with 200 mL portions of MC. Each organic extract was washed successively with two portions of 6M hydrochloric acid, water, saturated sodium bicarbonate solution and with water once more. The organic phase was combined and dried over anhydrous MgSO₄. After removal of solvent, the crude product was purified by column chromatography and recrystallized from hexane. 5.95 g (yield: 45%) of white crystals were obtained. ¹H-NMR (400 MHz, CDCl₃, ppm): δ 7.24 (s, 2H), 4.09~4.03 (t, *J* = 6.5 Hz, 4H), 1.88~1.8 (m, 4H), 1.49~1.42 (m, 4H), 1.36~1.25 (m, 24H), 0.88~0.84 (t, *J* = 6.5 Hz, 6H). ¹³C-NMR (100 MHz, CDCl₃, ppm): δ 169.12, 154.80, 126.51, 107.32, 70.45, 32.75, 30.43, 30.4, 30.18, 30.16, 29.7, 26.75, 23.53, 14.96.

III-2-1-4. 4,5-Bis-decyloxy-phthalic acid (4)^[38]

A mixture of 4,5-dicyano-1,2-bis-decyloxy-benzene (5.95 g, 13.5 mmol), 10% NaOH (50 mL) and ethanol (15 mL) were stirred at 80 °C for 2 hours. After being cooled, the resulting mixture acidified with concentrated hydrochloric acid. The white solid was collected by filtration, washed with distilled water and dried at 60 °C. 5.56 g (yield: 86%) of white solid was obtained. ¹H-NMR (400 MHz, DMSO-*d*₆, ppm): δ 7.53 (2, 2H), 7.37 (s, 2H), 4.02~3.99 (t, *J* = 6.2 Hz, 4H), 1.74~1.67 (m, 4H), 1.46~1.39 (m, 4H), 1.33~1.25 (m, 24H), 0.86~0.83 (t, *J* = 6.6 Hz, 6H). ¹³C-NMR (100 MHz, CDCl₃, ppm): δ 170.31, 154.75, 127.04, 108.06, 70.86, 33.07, 30.68, 30.56, 30.27, 30.19, 29.73, 26.74, 23.92, 15.08.

III-2-1-5. 2-Butyl-5,6-bis-decyloxy-isoindole-1,3-dione (5)³⁹¹

4,5-Bis-decyloxy-phthalic acid (5.27 g, 11 mmol) was dissolved in acetic acid (40 mL) and then n-butylamine (5.45 mL, 55 mmol) was added. The mixture was heated at reflux for overnight under an atmosphere of dry nitrogen. After the reaction mixture was cooled to room temperature, water and EA were added. The aqueous phase was extracted with EA and combined organic layer was dried over MgSO₄. The solvent was removed under vacuum and the residue was purified by column chromatography (silica gel, hexane:ether 10:1 v/v). 4.82 g (yield: 85%) of white solid was obtained. ¹H-NMR (400 MHz, CDCl₃, ppm): δ 7.23 (s, 2H), 4.08~4.05 (t, *J* = 6.6 Hz, 4H), 3.62~3.59 (t, *J* = 6.6 Hz, 2H), 1.87~1.8 (m, 4H), 1.64~1.59 (m, 2H), 1.49~1.42 (m, 4H), 1.36~1.23 (m, 26H), 0.93~0.9 (t, *J* = 7.4 Hz, 4H), 0.88~0.84 (t, *J* = 6.6 Hz, 6H). ¹³C-NMR (100 MHz, CDCl₃, ppm): δ 169.87, 154.59, 126.20, 107.53, 70.57, 38.72, 32.91, 31.83, 30.72, 30.59, 30.55, 30.34, 29.91, 26.92, 23.69, 21.08, 15.11, 14.68.

III-2-1-6. 4,7-Dibromo-2-butyl-5,6-bis-decyloxy-isoindole-1,3-dione (6)

2-Butyl-5,6-bis-decyloxy-isoindole-1,3-dione (4.64 g, 9 mmol) was dissolved in a mixture of sulfuric acid (H₂SO₄, 14 mL) and trifluoroacetic acid (TFA, 46 mL). The solution was kept in the dark. NBS (4.81 g, 27 mmol) was added in four portions and the reaction mixture was stirred at room temperature for overnight. The brown-red solution was poured into water and extracted with dichloromethane. The organic phases were combined and dried over anhydrous MgSO₄. The solvent was removed under reduced pressure and the crude product was purified by column chromatography using MC:hexane as the eluent (ratio 3:2 v/v) to afford 4.55 g of the product as white powder (Yield = 75%). ¹H-NMR (400 MHz, CDCl₃, ppm): δ 4.08~4.05 (t, *J* = 6.6 Hz, 4H), 3.66~3.63 (t, *J* = 7.4 Hz, 2H), 1.85~1.78 (m, 4H), 1.66~1.59 (m, 2H), 1.51~1.44 (m, 4H), 1.38~1.25 (m, 26H), 0.94~0.9 (t, *J* = 7.4 Hz, 4H), 0.88~0.84 (t, *J* = 6.6 Hz, 6H). ¹³C-NMR (100 MHz, CDCl₃, ppm): δ 165.95, 156.69, 127.93, 115.76, 75.89, 39.35, 32.92, 31.44, 31.14, 30.74, 30.59, 30.40, 30.34, 26.95, 23.70, 21.07, 15.12, 14.61.

III-2-1-7. 2-Butyl-5,6-bis-decyloxy-4,7-di-thiophen-2-yl-isoindole-1,3-dione (7)

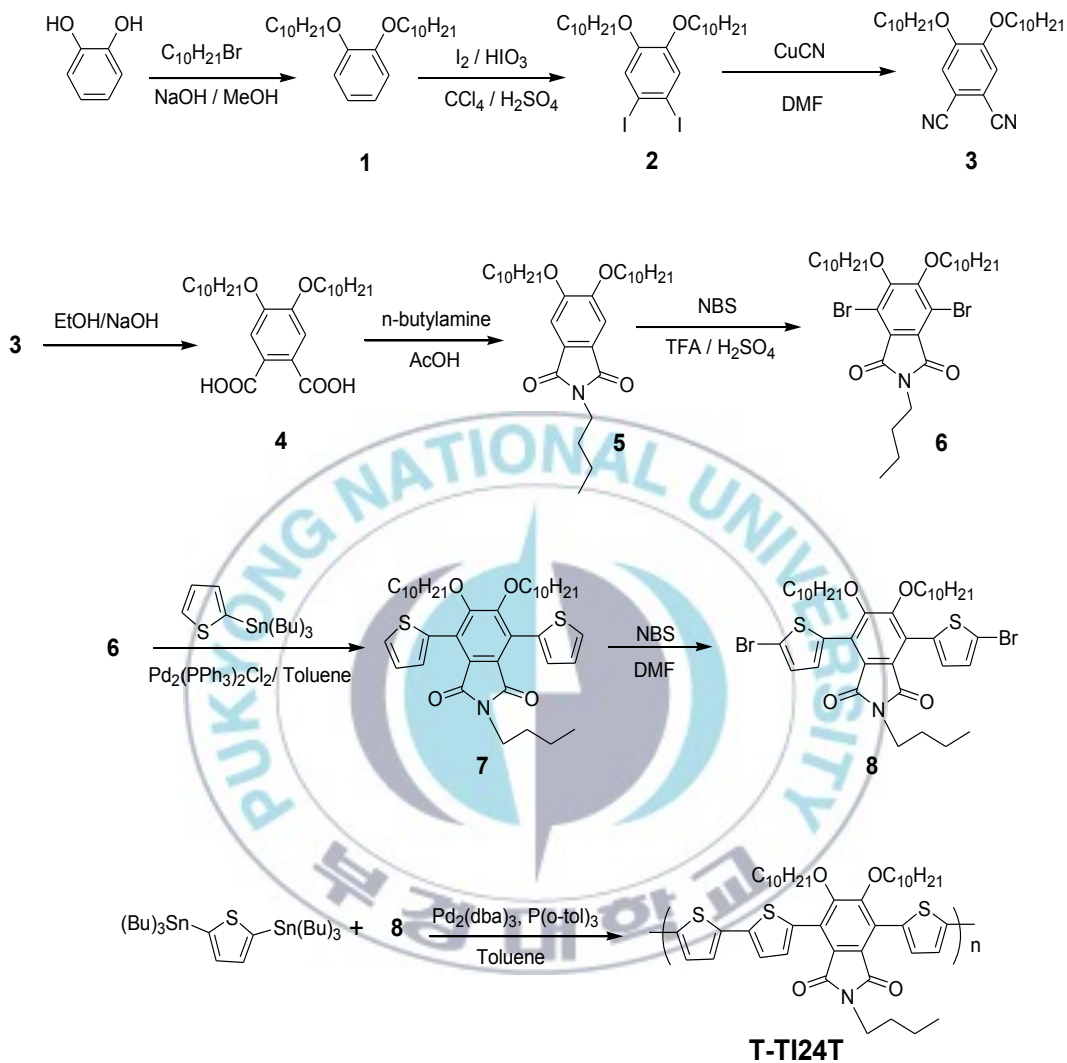
A mixture of 4,7-dibromo-2-butyl-5,6-bis-decyloxy-isoindole-1,3-dione (4.04 g, 6 mmol), 2-tributylstannylthiophene (5.6 g, 15 mmol), [1,1'-bis(diphenylphosphino) ferrocene] dichloropalladium (II), complex with dichloromethane ($\text{Pd}(\text{dppf})\text{Cl}_2 \cdot \text{CH}_2\text{Cl}_2$, 0.245 g, 0.3 mmol) was dissolved in dry toluene (30 mL) and then the reaction mixture was heated under reflux for 16 hours under N_2 . After the reaction mixture was cooled to room temperature, water and EA were added. The aqueous phase was extracted with EA and combined organic layer was dried over MgSO_4 . The solvent was removed under vacuum and the residue was purified by column chromatography (silica gel, hexane:MC, 10:1 v/v) affording a yellow oil (3.06 g, 75%). $^1\text{H-NMR}$ (400 MHz, CDCl_3 , ppm): δ 7.51~7.49 (dd, $J_1 = 1.1$ Hz, $J_2 = 5.2$ Hz, 2H), 7.29~7.28 (dd, $J_1 = 1.1$ Hz, $J_2 = 3.3$ Hz, 2H), 7.15~7.13 (t, $J = 3.7$ Hz, 2H), 3.87~3.84 (t, $J = 6.6$ Hz, 4H), 3.53~3.50 (t, $J = 7.7$ Hz, 2H), 1.58~1.53 (m, 6H), 1.3~1.22 (m, 36H), 0.94~0.86 (m, 9H). $^{13}\text{C-NMR}$ (100 MHz, CDCl_3 , ppm): δ 167.59, 156.66, 132.20, 131.17, 129.51, 128.48, 127.48, 126.79, 75.48, 38.90, 32.94, 31.52, 31.04, 30.96, 30.61, 30.58, 30.37, 26.78, 23.72, 21.20, 15.15, 14.65.

III-2-1-8. 4,7-Bis-(5-bromo-thiophen-2-yl)-2-butyl-5,6-bis-decyloxy-isoindole-1,3-dione (8)

2-Butyl-5,6-bis-decyloxy-4,7-di-thiophen-2-yl-isoindole-1,3-dione (2.72 g, 4 mmol) was dissolved in DMF (40 mL). The reaction mixture was then placed in ice-bath, and NBS (1.78 g, 10 mmol) was added. The reaction mixture was then stirred in dark for 24 hours, with the temperature being gradually raised to room temperature. The reaction mixture was then extracted with EA and excess of water (to remove NBS and DMF). The ethyl acetate layer was dried over MgSO₄ and the solvent was removed under reduced pressure, and the residue was chromatographically purified on silica gel column eluting with MC:hexane (1:10 v/v) as yellow oil (3.02 g, 90%). ¹H-NMR (400 MHz, CDCl₃, ppm): δ 7.12~7.11 (d, *J* = 3.7 Hz, 2H), 7.09~7.08 (d, *J* = 3.7 Hz, 2H), 3.91~3.88 (t, *J* = 6.2 Hz, 4H), 3.56~3.52 (t, *J* = 7.3 Hz, 2H), 1.63~1.52 (m, 6H), 1.34~1.25 (m, 36H), 0.9~0.85 (m, 9H). ¹³C-NMR (100 MHz, CDCl₃, ppm): δ 167.37, 156.37, 133.48, 131.91, 130.36, 128.68, 126.61, 115.78, 75.65, 39.01, 32.93, 31.50, 31.04, 30.95, 30.61, 30.59, 30.37, 26.84, 23.71, 21.19, 15.14, 14.64.

III-2-1-9. Synthesis of Polymer T-TI24T

4,7-Bis-(5-bromo-thiophen-2-yl)-2-butyl-5,6-bis-decyloxy-isoindole-1,3-dione (167.562 mg, 0.2 mmol), 2,5-bis(tributylstannyl)thiophene (0.2 mmol, 132.45 mg), Pd₂dba₃ (9.1572 mg, 10 μmol) and tri-(o-tolyl)phosphine (24.3496 mg, 8 μmol) was mixed in dry degassed toluene (6 mL). The reaction mixture was heated to reflux for 48 hours under nitrogen. After cooling to room temperature, ammonia water and dilute aqueous HCl were added to the mixture and the reaction mixture was stirred at room temperature overnight. The reaction mixture was then extracted with water and chloroform. The chloroform layer was dried over MgSO₄, concentrated by rotary evaporator and the reaction mixture was poured into methanol and the polymer was allowed to precipitate. The polymer was filtered and purified by Soxhlet extraction using methanol, hexane, respectively. Drying in vacuum afforded polymer. Yield: 114.02 mg (75%), reddish orange solid.



Scheme III-1. Synthesis of monomer and polymer (T-TI24T).

III-2-2. Fabrication of Device

Bulk heterojunction solar cells using polymer T-TI24T as a donor material and PC₆₁BM as an acceptor material were fabricated with a structure of ITO/PEDOT:PSS/active layer/Al. The ITO-glass substrates were pre-cleaned with deionized water, acetone, methanol, 2-propanol in ultrasonic bath. Then the substrates were dried on a hot-plate at 150 °C for 10 min and treated by UV/O₃ for 120 sec. A layer (~40 nm) of diluted poly(3,4-ethylenedioxythiophene):poly(styrenesulfonate) (PEDOT:PSS, Clevios P) with 2-propanol (PEDOT:2-propanol = 1:2 by volume) was spin-coated on ITO substrate (sheet resistance = 15 Ω/sq). After being baked at 150 °C for 10 min under the air, active layer was spin-cast from the blend solution of polymer/PCBM at 600 rpm for 120 s. The blend of polymer (concentration of polymer was kept at 15 mg/mL) and PCBM with different weight ratios were dissolved in o-dichlorobenzene (DCB). The blended solution was stirred for overnight at 60 °C in the glove box. Prior to spin coating, the active solution was filtered through 0.45 μm membrane filter. Then, the aluminum cathode deposited with a thickness of 110 nm through a shadow mask with a device area of 0.13 cm² at 2 x 10⁻⁶ Torr.

III-2-3. Measurement

Synthesized compounds were characterized by $^1\text{H-NMR}$ and $^{13}\text{C-NMR}$ spectrum, which were obtained with a JEOL JNM ECP-400 spectrometer. Gel permeation chromatography (GPC) measurements were conducted by GPC system equipped with a Varian 212-LC pump, a Rheodyne 6-port sample injection valve, a Waters Temperature Control Module, a Waters 410 differential RI detector and two Waters Styragel HR4E columns using polystyrene as standard and toluene as eluent. The thermogravimetric analysis (TGA) was carried out under the N_2 atmosphere at a heating rate of $10\text{ }^\circ\text{C}/\text{min}$ with a Perkin-Elmer TGA 7 thermal analyzer. The UV-Vis spectrum was recorded using a JASCO V-530 UV-Vis Spectrophotometer. The cyclic voltammetry (CV) was performed by an Ivium B14406 with a three electrode cell in a solution of Bu_4NPF_6 (0.1 M) in mixture of freshly distilled MC and DCB (1:1 v/v) at a scan rate of $100\text{ mV}/\text{s}$. Pt wires were used as the counter and working electrode and a Ag/Ag^+ electrode was used as the reference electrode. The J - V measurements under the 1.0 sun ($100\text{ mW}/\text{cm}^2$) condition from a 150 W Xe lamp with AM 1.5G filter were performed using a KEITHLEY Model 2400 source measure unit. A calibrated Si reference cell with a KG5 filter certified by National Institute of Advanced Industrial Science and Technology was used to confirm 1.0 sun

condition. The thickness of films was measured by an Alpha-Step IQ surface profiler (KLA-Tencor Co.).

III-3. Results and Discussion

III-3-1. Thermal Properties

The thermal property of the polymer was investigated by thermogravimetric analyses (TGA), and its thermogram is depicted in Figure III-2. The 5% weight-loss temperature (T_d) of T-TI24T was 380 °C. It exhibited good thermal stability against oxygen-an important characteristic for device fabrication and application.

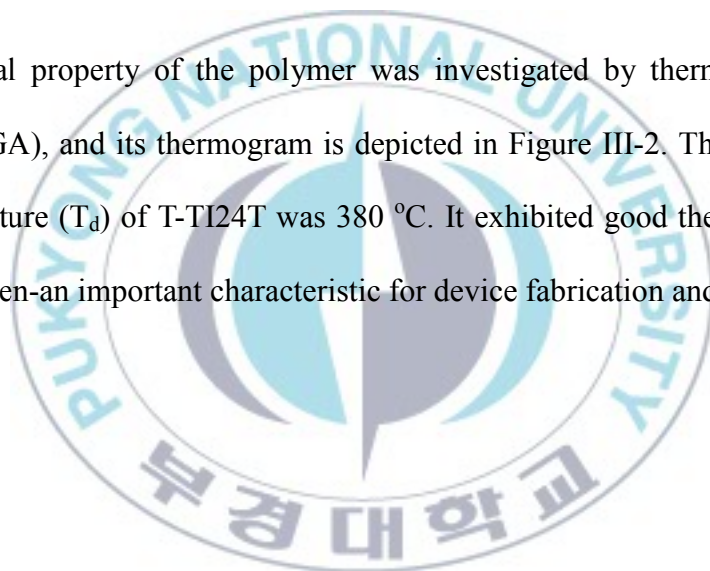


Table III-2. Molecular weight and thermal properties of T-TI24T.

Polymer	M_n (g/mol)	M_w (g/mol)	PDI	T_d ($^{\circ}\text{C}$)
T-TI24T	86,500	117,800	1.36	380

M_n : The number average molecular weight

M_w : The weight average molecular weight

PDI: Polydispersity indexes

M_n , M_w and PDI determined by GPC in Toluene on the basis of polystyrene calibration.

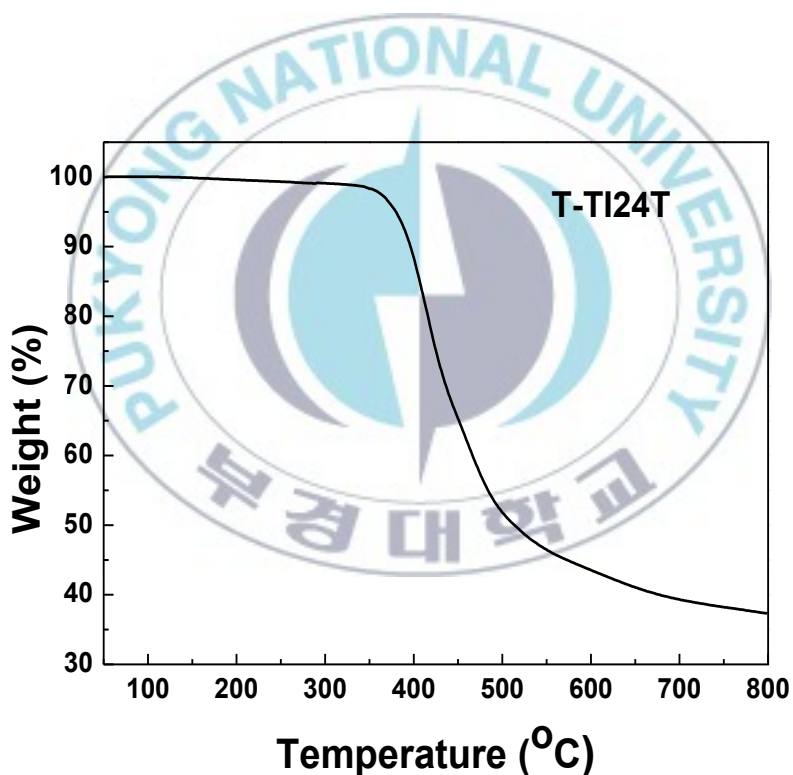


Figure III-2. TGA thermogram of polymer T-TI24T with a heating rate of $10\text{ }^{\circ}\text{C min}^{-1}$ under a N_2 atmosphere.

III-3-2. Optical Properties

The photo-physical characteristic of the polymer was investigated by UV-Vis absorption spectroscopy in spin-coated film on glass substrate. The UV-Vis absorption spectra of T-TI24T thin solid film coated from DCB solution is depicted in Figure III-3 and Table III-3 lists the optical properties of the polymer. A maximum UV-Vis absorption peak (λ_{\max}) appeared at 456 nm. The UV-Vis absorption range of T-TI24T was not wide in comparison with other DA-type polymers based on typical electron-withdrawing moiety 2,1,3-benzothiadiazole with various electron-donating moieties such as fluorene derivative (PF-TBT), carbazole derivative (PCD-TBT) or cyclopentadithiophene (PCPD-TBT). Generally, band gap energy of DA-type polymer which comprises of an electron-rich “donor” moiety and an electron-deficient “acceptor” moiety is effectively decreased by orbital overlap through internal charge transfer between electron-donating materials and electron-withdrawing materials. Therefore, in DA-type polymer back-bone, the stronger electron-withdrawing property of electron-deficient material leads to the narrower the band gap. The optical band gap (E_g^{opt}) value of T-TI24T estimated from the absorption edge in the UV-Vis spectrum of the thin solid film was 2.24 eV.

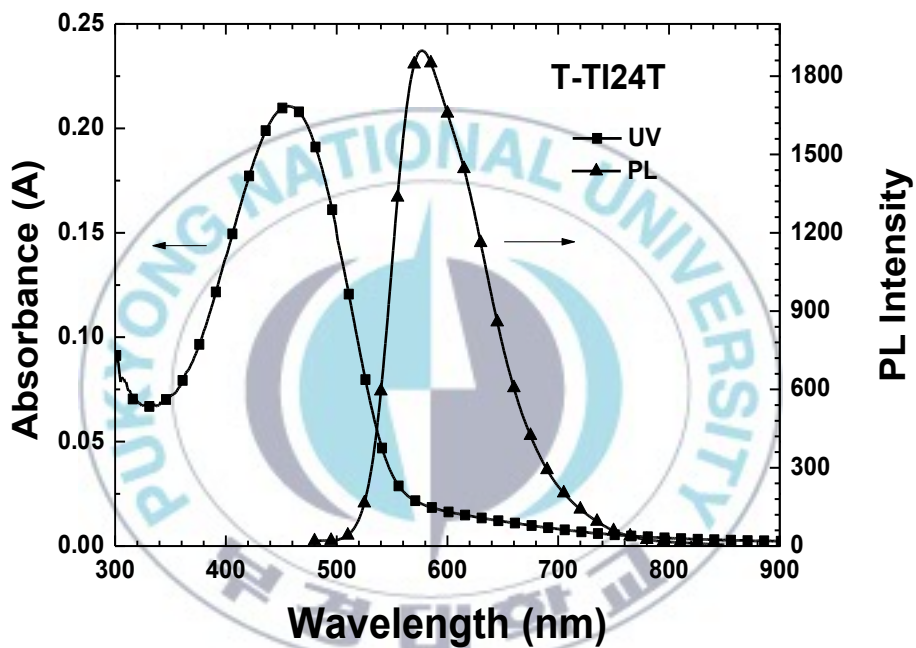


Figure III-3. UV-Vis absorption and PL spectrum of T-Ti24T film.

III-3-3. Electrochemical Properties

Cyclic voltammetry was usually applied to estimate the HOMO and LUMO energy levels of conjugated polymers. The onset oxidation and reduction potentials obtained from cyclic voltammogram correspond to HOMO and LUMO energy levels, respectively. The HOMO and LUMO levels figured out from the oxidation and reduction onset potential of cyclic voltammogram (Figure III-4) were -5.33 and -3.8 eV, respectively. It should be noted that the HOMO energy level of T-TI24T was relatively low in comparison with other photovoltaic polymers based on thiophene derivatives such as polymers based on thiophene combined with various electron-deficient moieties 2,1,3-benzothiadiazole, 2,1,3-benzooxadiazole, 2,1,3-benzotriazole or polymers based on thiophene derivatives and diketopyrrolopyrrole.^[30] Since the V_{oc} value of BHJ solar cell was directly related to the energy difference between the HOMO level of the donor polymer and the LUMO level of the acceptor, it was expected that T-TI24T would exhibit high V_{oc} values in the final device. The electrochemical band gap (E_g^{CV}) of T-TI24T was 2.15 eV, and this was determined by the difference between the HOMO and the LUMO energy levels. The optical and electrochemical properties of the polymers are summarized in Table III-3.

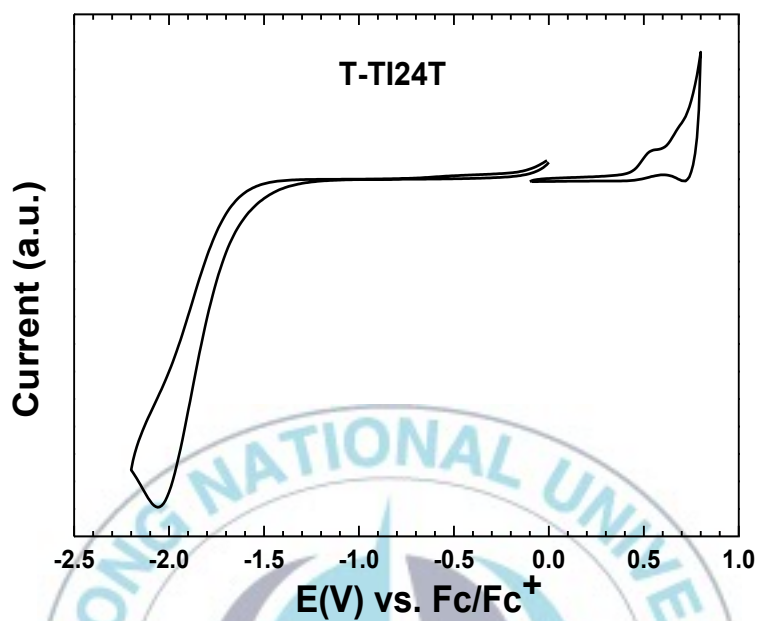


Figure III-4. Cyclic voltammogram of T-TI24T in an MC:DCB (1:1 v/v) of 0.1 M Bu_4NPF_6 .

Table III-3. Optical absorption and electrochemical properties of T-TI24T.

Polymer	λ_{max} (nm)	PL_{max} (nm)	$E_{\text{g}}^{\text{opt}}$ (eV)	HOMO (eV)	LUMO (eV)	E_{g}^{cv} (eV)
T-TI24T	456	577	2.24	-5.33	-3.15	2.15

III-3-4. Photovoltaic Properties

BHJ solar cells using T-TI24T as donor material and PC₆₁BM as an acceptor material were fabricated with a structure of ITO/PEDOT:PSS/active layer/ Al. Devices were fabricated from different weight ratios of T-TI24T/PC₆₁BM and the concentration of polymer solution was kept at 15 mg/mL. A comparison of devices with different weight ratios of donor/acceptor was depicted in Figure III-5 and Table III-4. When the ratio of T-TI24T/PC₆₁BM increased from 1:1 to 1:3, the J_{sc} , V_{oc} , FF and PCE of devices increased. The ratio between the polymer and the fullerene in bulk heterojunction devices is of great importance in terms of photovoltaic response and the optimum ratio depends on the type of polymer and the morphology is affected by ratio between the polymer and PC₆₁BM. The best PCE of 0.199% was exhibited in the device with T-TI24T/PC₆₁BM = 1:3 (w/w). This device exhibits a relatively high value of V_{oc} of 0.99 V, which is contributed from a relatively low-lying HOMO energy level of polymer. All of devices show low J_{sc} (0.23-0.76 mA/cm²) which could be related to a narrow absorption spectrum of T-TI24T. The PCE of devices were governed by the J_{sc} value and FF which are primarily determined by the photon absorption property and charge carrier mobility.

Table III-4. Photovoltaic properties of T-TI24T.

Active layer	Weight ratio (w/w)	Thickness (nm)	J_{sc} (mA/cm ²)	V_{oc} (V)	FF (%)	PCE (%)
T-TI24T: PC ₆₁ BM	1:1	80	-0.23	0.6	25	0.035
	1:2	160	-0.53	0.94	26.9	0.134
	1:3	180	-0.76	0.99	26.5	0.199

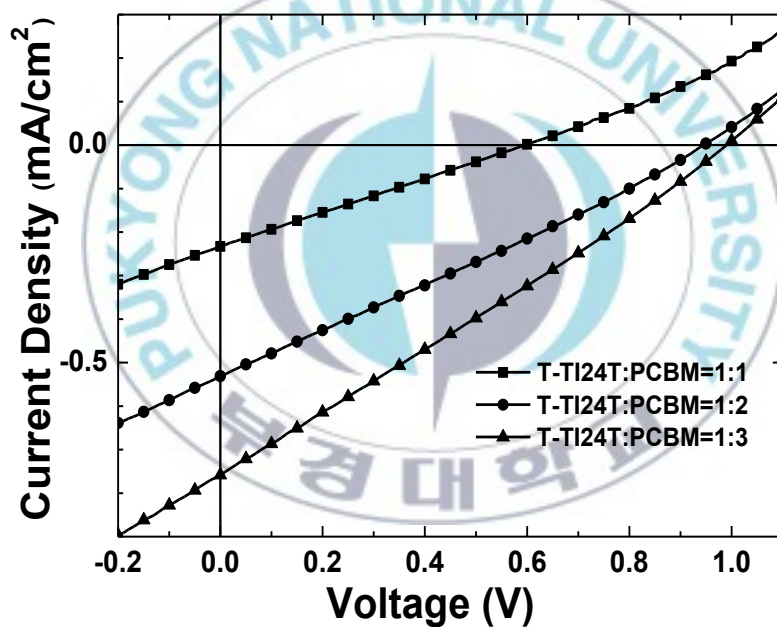


Figure III-5. J - V curves of conventional type OSCs based on T-TI24T under the illumination of AM 1.5G, 100 mW/cm².

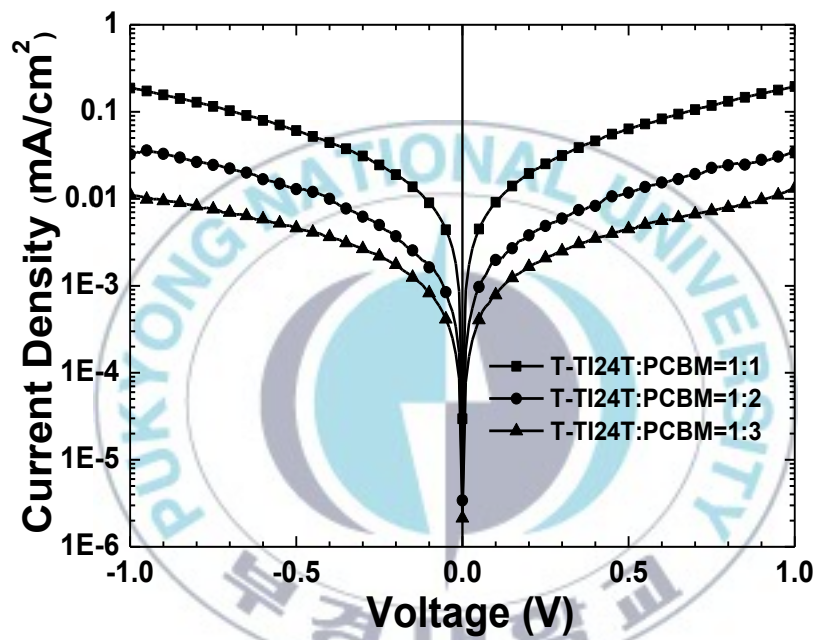
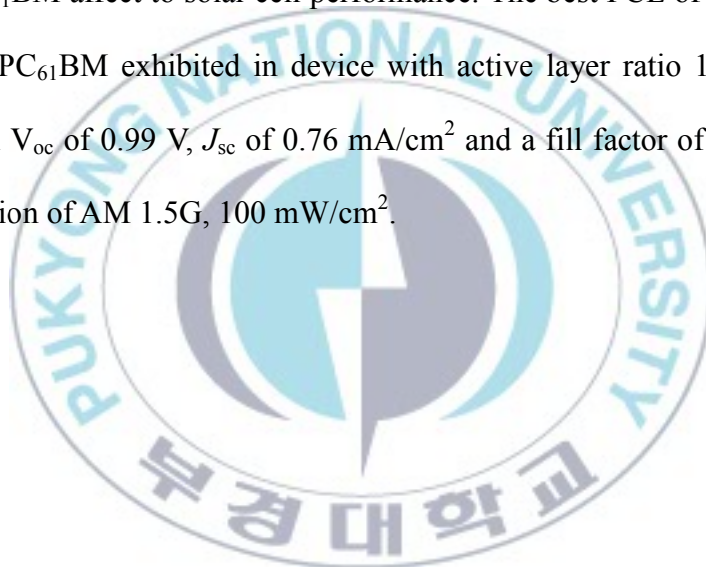


Figure III-6. *J*-*V* curves of conventional type OSCs based on T-TI24T under the dark condition.

III-4. Conclusion

The new D-A polymer T-TI24T was synthesized with high molecular weight, good and high thermal stability. Polymer has a maximum UV-Vis absorption peak at 456 nm. The HOMO and LUMO energy levels of the polymer determined by cyclic voltammetry were -5.33 and -3.15 eV, respectively. The ratio of polymer/PC₆₁BM affect to solar cell performance. The best PCE of devices based on T-TI24T/PC₆₁BM exhibited in device with active layer ratio 1:3 (w/w) was 0.199% with V_{oc} of 0.99 V, J_{sc} of 0.76 mA/cm² and a fill factor of 26.5%, under the illumination of AM 1.5G, 100 mW/cm².



Chapter IV. Synthesis, Characterization and photovoltaic properties of π -Conjugated Polymers Based on Thiophene and 2,1,3-Benzoxadiazole Derivatives for Organic Solar Cells

IV-1. Introduction

For a conjugated polymer, HOMO level should be carefully tuned for several considerations. First of all, the HOMO energy level of a material, which describes the accessibility of the material molecule to be oxidized, reflects the air stability of the material. The oxidation threshold of air is ca. -5.2 eV against vacuum level. Therefore, the HOMO level cannot be more positive than this value to provide the air stability to the polymer. Secondly, the maximum V_{oc} is correlated to the difference between the LUMO energy level of PCBM and the polymer's HOMO energy level based on experimental. Therefore, in order to achieve high V_{oc} in the device, HOMO level should be reasonably low.^[40-42] To adapt both of two requirements, the conjugated polymers should have strong electron-withdrawing units. With a proper selection of the acceptor, however, both the HOMO and LUMO energy level of the synthesized polymer can be decreased.^[7]

Benzothiadiazole (BT) is one of the strong electron withdrawing moieties widely used in OSCs due to their electron accepting strength as well as their

capability to adopt the quinoid structure in the polymer, resulting in a low-band gap and coplanar polymer.^[43, 44] Replacing the sulfur atom with an oxygen atom forms benzooxadiazole (BO), which can decrease both the HOMO and LUMO energy levels; this molecular structure not only can result in air-stable polymers but also produce high open-circuit potentials when blended with fullerenes.^[42] Besides, 5,6-bis alkoxy substitution of BO is very helpful for the construction of the conjugated polymers with better solubility and higher molecular weight, and meanwhile, the polymer chain could have a planar conformation, in comparison with the incorporation of BT. The good solubility of conjugated polymers is crucial for its purification and the formation of high-quality film for efficient optoelectronic devices.^[44]

In recent years-within two years, there have been some researches focused on synthesizing BO and applying to fabricating solar cell devices. Figure IV-1 and Table IV-1 summarize some structure, band gaps, HOMO levels and photovoltaic of conjugated polymer based on BO.

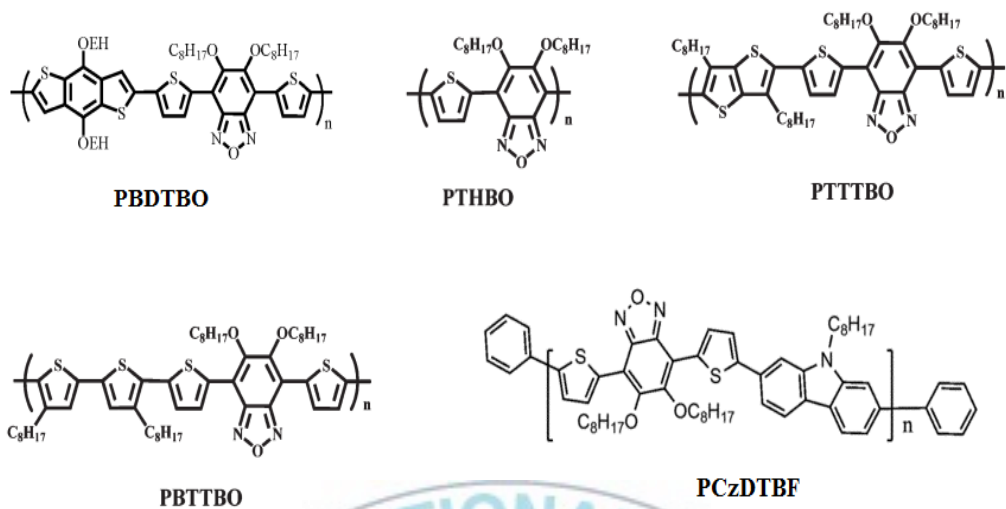
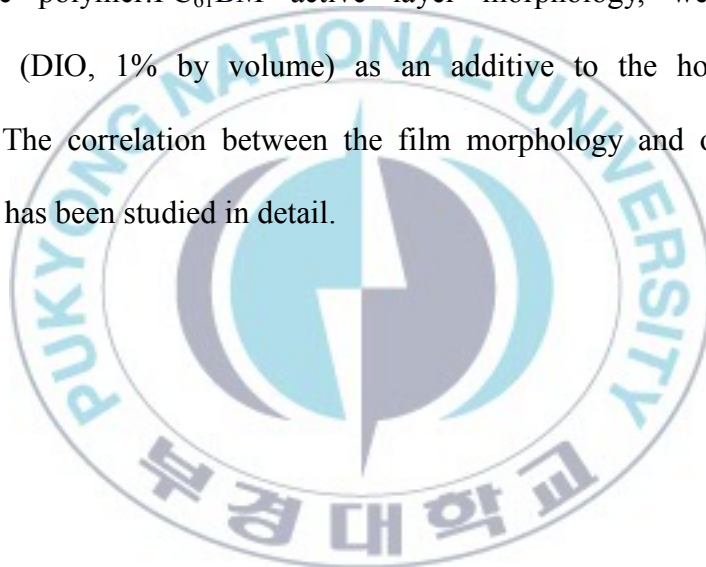


Figure IV-1. Chemical structures of copolymers based on BO.

Table IV-1. Summary of band gaps, HOMO levels, and photovoltaic properties of conjugated polymers based on BO.

Polymer	E_g^{opt} (eV)	HOMO (eV)	J_{sc} (mA/cm ²)	V_{oc} (V)	FF (%)	PCE (%)	Ref.
PTHBO	1.71	-5.47	8.3	1.02	51	4.2	42
PBTTBO	1.70	-5.13	6.9	0.74	72	3.7	42
PTTTBO	1.72	-5.28	10	0.87	58	5.1	42
PBDTBO	1.74	-5.27	10.4	0.86	64.4	5.7	43
PCzDTBF	1.93	-5.34	7.36	0.85	57	4.2	45

In this study, we synthesized a series of polymers based on BO derivatives namely 1T-BO20, 2T-BO20 and 3T-BO20 with different thiophene rings in donor and acceptor moieties to investigate the effect of the number of thiophene rings and their positions on optical, electrochemical and photovoltaic properties of polymers. Thiophene was used because it has been shown to have excellent optical and chemical stability in BHJ solar cells. On the other hand, in order to optimize the polymer:PC₆₁BM active layer morphology, we added 1,8-diodooctane (DIO, 1% by volume) as an additive to the host solvent of chloroform. The correlation between the film morphology and overall device performance has been studied in detail.



IV-2. Experimental Section

IV-2-1. Materials and Synthesis

Methylene chloride (MC) was distilled over CaH₂. All other chemicals were purchased from Sigma-Aldrich Co, Tokyo Chemical Industry (TCI) or Alfa Aesar (A Johnson Matthey Company) and used as received unless otherwise described.

IV-2-1-1. 1,2-Dinitro-4,5-bis-decyloxy-benzene (3)^[46]

1,2-Bis-decyloxy-benzene (9.766 g, 25 mmol) was dissolved in MC (150 mL) and acetic acid (AcOH, 150 mL). Then, the mixture was cooled to 10 °C and 65% nitric acid (30 mL) was added dropwise. The reaction was allowed to warm to room temperature and stirred for 1 hour. The mixture was again cooled to 10 °C and 100% nitric acid (70 mL) was added dropwise. The mixture was allowed to warm to room temperature and the mixture was stirred for 24 hours. After completion of the reaction, the reaction mixture was poured into ice-water and the MC layer separated. The water phase was extracted with MC. The combined organic phase was washed with water, sat. NaHCO₃ (aq), brine and dried over anhydrous MgSO₄. Concentration in vacuum gave the crude product that was recrystallized from methanol. Yield: 10.814 g (90%), yellow solid. ¹H-NMR (400

MHz, CDCl₃, ppm): δ 7.27 (s, 2H), 4.09~4.06 (t, J = 6.5 Hz, 4H), 1.88~1.81 (m, 4H), 1.49~1.42 (m, 4H), 1.34~1.25 (m, 24H), 0.87~0.84 (t, J = 6.5 Hz, 6H). ¹³C-NMR (100 MHz, CDCl₃, ppm): δ 152.81, 137.48, 108.92, 71.20, 32.87, 30.55, 30.51, 30.30, 30.21, 29.69, 26.80, 23.66, 15.07.

IV-2-1-2. 5,6-Bis-decyloxy-benzo[c][1,2,5]oxadiazole (4)

A mixture of 1,2-dinitro-4,5-bis-decyloxy-benzene (9.613 g, 20 mmol), sodium azide (NaN₃, 6.5 g, 100 mmol), and tetrabutyl ammonium bromide (n-Bu₄NBr, 1.29 g, 4 mmol) was heated under reflux in toluene (100 mL) for 12 hours under N₂ protection. Then, triphenyl phosphine (PPh₃, 6.295 g, 2.4 mmol) was added in small portions; when the PPh₃ was completely added, the mixture heated under reflux for an additional 24 hours. The reaction mixture was cooled to room temperature and filtered through a short silica plug; the plug was rinsed with hexane/MC. Evaporation of the solvents from the combined organic phases, under reduced pressure and afforded a crude solid that was recrystallized from methanol to yield a yellow solid (5.192 g, 60%). ¹H-NMR (400 MHz, CDCl₃, ppm): δ 6.78 (s, 2H), 4.06~4.02 (t, J = 6.6 Hz, 4H), 1.90~1.83 (m, 4H), 1.51~1.44 (m, 4H), 1.35~1.25 (m, 24H), 0.87~0.84 (t, J = 6.6 Hz, 6H). ¹³C-NMR (100 MHz, CDCl₃, ppm): δ 156.19, 147.82, 91.66, 70.35, 32.89, 30.57, 30.53, 30.32, 30.28, 29.58, 26.96, 23.66, 15.08.

IV-2-1-3. 4,7-Dibromo-5,6-bis-decyloxy-benzo[c][1,2,5]oxadiazole (5)

5,6-Bis-decyloxy-benzo[c][1,2,5]oxadiazole (5.192 g, 12 mmol) was dissolved in a mixture of MC (200 mL) and acetic acid (100 mL) at room temperature. Bromine (4.5 mL, 87.4 mmol) was added and the resulting mixture was stirred in the dark for ca. 3 days at room temperature. An aqueous NaOH solution (10 g in 200 mL) was slowly poured into the reaction mixture. The aqueous phase was extracted with MC; the combined organic extracts were dried over anhydrous MgSO_4 and concentrated under reduced pressure to afford a crude solid that was purified through column chromatography (SiO_2 , hexane:MC with ratio 9:1 v/v) to yield a white solid (5.6 g, 79%). $^1\text{H-NMR}$ (400 MHz, CDCl_3 , ppm): δ 4.13~4.10 (t, $J = 6.6$ Hz, 4H), 1.87~1.80 (m, 4H), 1.52~1.45 (m, 4H), 1.34~1.25 (m, 24H), 0.87~0.84 (t, $J = 6.2$ Hz, 6H). $^{13}\text{C-NMR}$ (100 MHz, CDCl_3 , ppm): δ 156.66, 148.44, 100.55, 76.39, 32.88, 31.18, 30.56, 30.55, 30.36, 30.30, 26.88, 23.66, 15.09.

IV-2-1-4. 5,6-Bis-decyloxy-4,7-di(thien-2-yl)benzo[c][1,2,5]oxadiazole (6)

4,7-Dibromo-5,6-bis-decyloxy-benzo[c][1,2,5]oxadiazole (5.313 g, 9 mmol), 2-tributylstannylthiophene (8.393 g, 22.5 mmol), [1,1'-bis(diphenylphosphino)ferrocene] dichloropalladium (II), complex with dichloromethane (Pd(dppf)Cl₂·CH₂Cl₂, 0.367 g, 0.45 mmol) were dissolved in dry toluene (50 mL) and then the reaction mixture was heated under reflux for overnight under N₂ atmosphere. After the reaction mixture was cooled to room temperature, water and EA were added. The aqueous phase was extracted with EA and combined organic layer was dried over anhydrous MgSO₄. The solvent was removed under vacuum and the residue was purified by column chromatography (silica gel, hexane:CF₃, 10:1 v/v) afforded a yellow solid (3.76 g, 70%). ¹H-NMR (400 MHz, CDCl₃, ppm): δ 8.45~8.44 (dd, *J*₁ = 1.1 Hz, *J*₂ = 3.7 Hz, 2H), 7.49~7.41 (dd, *J*₁ = 1.1 Hz, *J*₂ = 5.2 Hz, 2H), 7.21~7.19 (t, 4.6 Hz, 2H), 4.15~4.11 (t, *J* = 11.0 Hz, 4H), 2.02~1.94 (m, 4H), 1.48~1.41 (m, 4H), 1.37~1.26 (m, 24H), 0.89~0.85 (t, *J* = 6.6 Hz, 6H). ¹³C-NMR (100 MHz, CDCl₃, ppm): δ 152.69, 147.74, 133.90, 131.85, 129.00, 128.14, 114.05, 75.50, 32.92, 31.28, 30.62, 30.58, 30.56, 30.35, 26.88, 23.69, 15.11.

IV-2-1-5. 4,7-Bis(5-bromothien-2-yl)-5,6-bis-decyloxy-benzo[c][1,2,5]oxadiazole (7)

5,6-Bis-decyloxy-4,7-di(thien-2-yl)benzo[c][1,2,5]oxadiazole (3.58 g, 6 mmol) was dissolved in DMF (40 mL). The reaction mixture was then placed in ice-bath, and NBS (2.67 g, 15 mmol) was added. The reaction mixture was then stirred in dark for 24 hours, with the temperature being gradually raised to room temperature. Water and NaHSO₃ were added into the reaction mixture and stirred for 20 min to remove NBS. The mixture was then extracted with EA. The organic layer was combined and dried over anhydrous MgSO₄ and the solvent was removed under reduced pressure, and the residue was chromatographically purified on silica gel column eluting with MC:hexane (1:10 v/v) as a reddish orange solid (4.08 g, 90%). ¹H-NMR (400 MHz, CDCl₃, ppm): δ 8.22~8.21 (d, *J* = 4.0 Hz, 2H), 7.15~7.14 (d, *J* = 4.4 Hz, 2H), 4.15~4.11 (t, *J* = 7.4 Hz, 4H), 2.0~1.93 (m, 4H), 1.47~1.41 (m, 4H), 1.36~1.27 (m, 24H), 0.89~0.85 (t, *J* = 6.6 Hz, 6H). ¹³C-NMR (100 MHz, CDCl₃, ppm): δ 152.27, 147.23, 135.31, 132.21, 131.09, 117.39, 113.71, 75.83, 32.99, 31.24, 30.09, 30.65, 30.55, 30.43, 26.89, 23.77, 15.19.

IV-2-1-6. Synthesis of polymers (1T-BO20, 2T-BO20 and 3T-BO20)

Compound 5 (118.086 mg, 0.2 mmol) or compound 7 (150.936 mg, 0.2 mmol), 2,5-bis(tributylstannyl)thiophene (132.45 mg, 0.2 mmol) or 5,5'-bis(tributylstannyl)-2,2'-bithiophene (148.87 mg, 0.2 mmol), Pd₂dba₃ (9.1572 mg, 10 μmol) and tri-(o-tolyl)phosphine (24.3496 mg, 8 μmol) were mixed in dry degassed toluene (6 mL). The reaction mixture was heated to reflux for 48 hours (for 1T-BO20 and 3T-BO20) or 20 min (for 1T-BO20) under nitrogen. After cooling to room temperature, the mixture was poured into 200 mL methanol and the polymer was allowed to precipitate. The polymer was filtered and purified by Soxhlet extraction using methanol, hexane and chloroform. The chloroform fraction was concentrated by rotary evaporator and then poured into methanol to precipitate again. The polymer was filtered and dried in vacuum. Yield: 1T-BO20 82.04 mg (80%), 2T-BO20 41.64 mg (35%), and 3T-BO20 67.7 mg (50%) as dark solids.

IV-2-2. Fabrication of Device

Bulk heterojunction solar cells using polymers 1T-BO20, 2T-BO20, 3T-BO20 as donor materials and PC₆₁BM as an acceptor material were fabricated with a structure of ITO/PEDOT:PSS/active layer/Al. The ITO-glass substrates were pre-cleaned with deionized water, acetone, methanol, 2-propanol in ultrasonic bath. Then the substrates were dried on a hot-plate at 150 °C for 10 min and treated by UV/O₃ for 120 sec. A layer (~40 nm) of diluted poly(3,4-ethylenedioxythiophene):poly(styrenesulfonate) (PEDOT:PSS, Clevis P) with 2-propanol (PEDOT:2-propanol = 1:2 by volume) was spin-coated on ITO substrate (sheet resistance = 15 Ω/sq). After being baked at 150 °C for 10 min under the air, active layer was spin-cast from the blend solution of polymer/PCBM at 600 rpm for 120 s. The blend of 5 mg of polymer and 10 mg of PCBM were dissolved in 1 mL of chloroform (CF) or 1 mL of CF with 1% v/v of DIO. The blended solution was stirred for overnight at 40 °C in the glove box. Prior to spin coating, the active solution was filtered through 0.45 μm membrane filter. Then, the aluminum cathode deposited with a thickness of 110 nm through a shadow mask with a device area of 0.13 cm² at 2 x 10⁻⁶ Torr.

IV-2-3. Measurement

Synthesized compounds were characterized by $^1\text{H-NMR}$ and $^{13}\text{C-NMR}$ spectrum, which were obtained with a JEOL JNM ECP-400 spectrometer. Gel permeation chromatography (GPC) measurements were conducted by GPC system equipped with a Varian 212-LC pump, a Rheodyne 6-port sample injection valve, a Waters Temperature Control Module, a Waters 410 differential RI detector and two Waters Styragel HR4E columns using polystyrene as standard and toluene as eluent. The thermogravimetric analysis (TGA) was carried out under the N_2 atmosphere at a heating rate of $10\text{ }^\circ\text{C}/\text{min}$ with a Perkin-Elmer TGA 7 thermal analyzer. The UV-Vis spectrum was recorded using a JASCO V-530 UV-Vis Spectrophotometer. Atomic Force Microscope (AFM) images were taken on a Digital Instruments (U.S.A), Multi ModeTM SPM. AFM images were obtained by the tapping mode and a scan rate of 2 Hz . The cyclic voltammetry (CV) was performed by an Ivium B14406 with a three electrode cell in a solution of Bu_4NPF_6 (0.1 M) in acetonitrile at a scan rate of 100 mV/s . Pt wires were used as the counter and working electrode coated polymers and a Ag/Ag^+ electrode was used as the reference electrode. The J - V measurements under the 1.0 sun ($100\text{ mW}/\text{cm}^2$) condition from a 150 W Xe lamp with AM 1.5 G filter were performed using a KEITHLEY Model 2400 source-measure unit. A calibrated Si reference cell with a KG5 filter certified by National Institute of

Advanced Industrial Science and Technology was used to confirm 1.0 sun condition. The thickness of films was measured by an Alpha-Step IQ surface profiler (KLA-Tencor Co.).

IV-3. Results and Discussion

IV-3-1. Thermal Properties

All the polymers exhibited good thermal stability with 5% weight-loss temperatures (T_d). T_d values of 1T-BO20, 2T-BO20 and 3T-BO20 were 308, 279 and 309 °C, respectively (see Figure IV-2). The high thermal stability of the resulting polymers prevents the deformation of the polymer morphology and the degradation of active layer applied in OSCs. Besides, this result suggested that the number of thiophene units along the polymer backbone did not affect the thermal stability of the polymers.

Table IV-2. Molecular weight and thermal properties of 1T-BO20, 2T-BO20 and 3T-BO20.

Polymer	M _n (g/mol)	M _w (g/mol)	PDI	T _d (°C)
1T-BO20	68,500	118,700	1.73	308
2T-BO20	11,500	87,300	7.61	279
3T-BO20	36,600	60,800	1.66	309

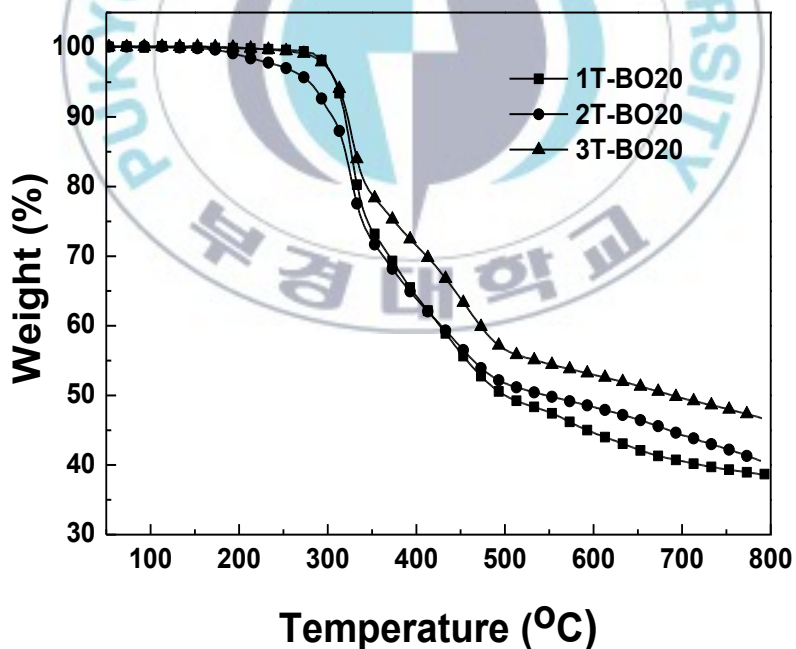


Figure IV-2. TGA thermogram of polymers 1T-BO20, 2T-BO20 and 3T-BO20 with a heating rate of 10 °C min⁻¹ under a N₂ atmosphere.

IV-3-2. Optical Properties

The normalized UV–Vis absorption spectra of 1T-BO20, 2T-BO20 and 3T-BO20 films spin-coated from a 10 mg/mL DCB solution are shown in Figure IV-3, and the main optical properties are listed in Table IV-3. All of the absorption spectra recorded from polymer films feature two absorption bands: one at 310-460 nm which we assign to localized π - π^* transition of the conjugated polymer backbone and another boarder band from 460-740 nm in the long wavelength region, corresponding to intramolecular charge transfer (ICT) between the donor unit (thiophene or bithiophene) and BO-based acceptor. The maximum absorption peak at long wavelength of the 1T-BO20 film ($\lambda_{\text{max}} = 608, 663 \text{ nm}$) shows a red-shift of 6, 12 nm compared to 3T-BO20 ($\lambda_{\text{max}} = 602, 651 \text{ nm}$). Whereas the maximum absorption peak at long wavelength of 2T-BO20 ($\lambda_{\text{max}} = 611, 661 \text{ nm}$) is similar to 1T-BO20 because of the same chemical structure of the two polymers resulting in similar ICT effect. In addition, the absorption peak at short wavelength of 2T-BO20 (383 nm) and 3T-BO20 (408 nm) are red-shift 44 and 69 nm, respectively as compared with 1T-BO20 (339 nm). It means conjugated length was enhanced with the increasing number of thiophene rings in the repeating unit, which lead to an extension of the absorption spectrum of the polymer and thereby increasing light harvesting and consequently, performances of device.^[47] The optical band gap (E_g^{opt}) of three polymers (1T-BO20, 2T-BO20

and 3T-BO20) calculated from the absorption edges in the UV–Vis spectra of the thin solid films were 1.75, 1.78 and 1.72 eV, respectively. As expected, the low E_g^{opt} of BO-based D-A alternating high planar conjugated polymers, which is lower than that of P3HT homopolymer (~2.0 eV) is determined by strong π - π stacking and the ICT absorption bands.



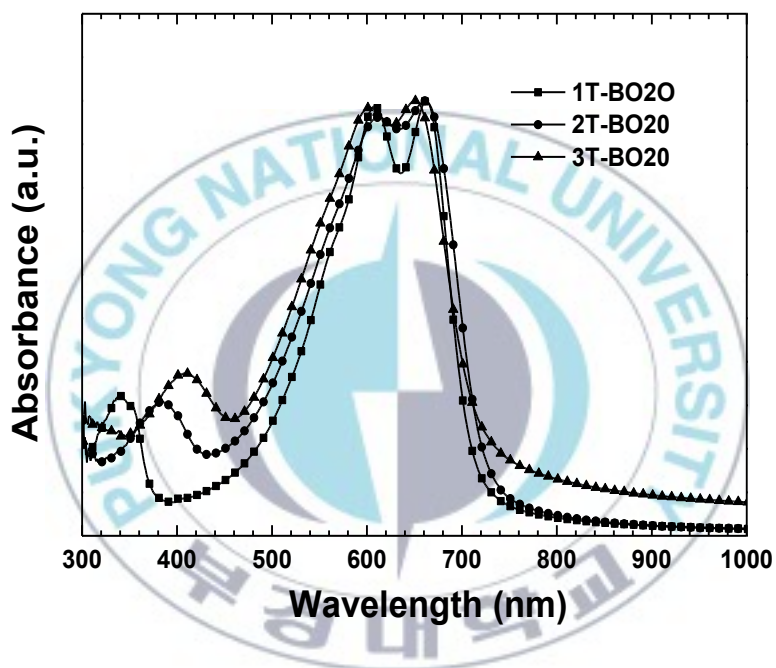


Figure IV-3. UV-Vis absorption spectra of 1T-BO₂O, 2T-BO₂O and 3T-BO₂O films.

IV-3-3. Electrochemical Properties

To investigate the band diagram of the polymers, and then understand the performance of the resulting solar cell devices, it is necessary to determine the energy levels of HOMO and LUMO of the polymers. Thus, the electrochemical behaviors of the polymers were investigated by CV measurements were carried out in acetonitrile solution containing 0.1 M Bu_4NPF_6 as the supporting electrolyte. The reference electrode (Ag/AgCl) was calibrated by the ferrocene/ferrocenium (Fc/Fc^+) redox couple (4.8 eV below the vacuum level). From the values of the onset oxidation potential and the onset reduction potential of the polymers, the HOMO and LUMO energy levels as well as the electrochemical band gaps were calculated.

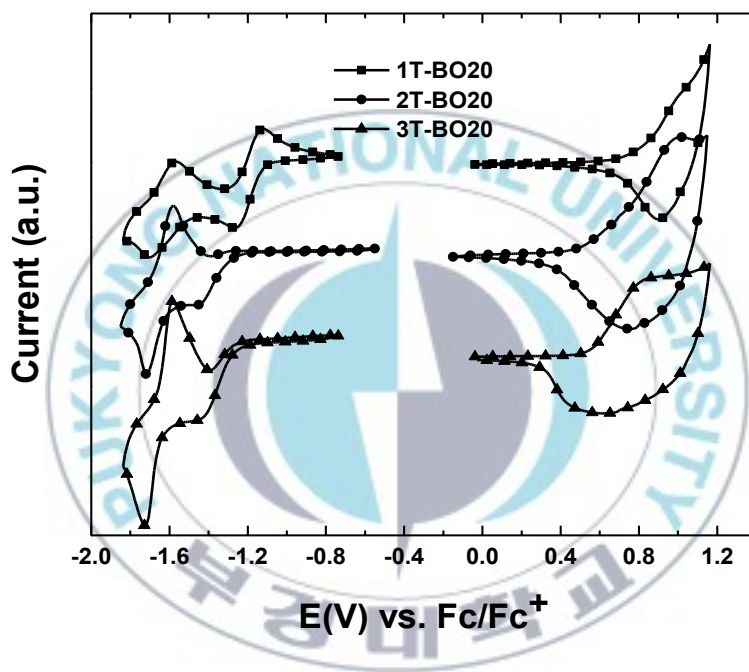


Figure IV-4. Cyclic voltammograms of 1T-BO20, 2T-BO20 and 3T-BO20.

The estimated HOMO and LUMO energy levels of polymers are compiled in Table IV-3. The HOMO energy levels of 1T-BO20, 2T-BO20 and 3T-BO20 were -5.53, -5.32 and -5.34 eV, respectively which are increased with enhancing of thiophene rings in both donor moiety (2T-BO20) and acceptor moiety (3T-BO20). The relatively low HOMO level of the polymers promised a V_{oc} value and good air stability for the photovoltaic cell. The LUMO energy levels of the polymers are in the order of 1T-BO20 (-3.68 eV) < 3T-BO20 (-3.5eV) < 2T-BO20 (-3.45 eV). This indicates that the LUMO energy levels are mainly determined by benzoxadiazole electron-acceptor contents in the polymer. That is to say, the π -electron-accepting ability decreases with increasing thiophene ring in donor moiety. Besides, the similar situation also happened when comparing HOMO levels of 1T-BO20 and 3T-BO20-with increasing of thiophene rings in the acceptor moiety. The E_g^{cv} of 1T-BO20, 2T-BO20 and 3T-BO20 estimated from the difference between the HOMO and LUMO energy levels were 1.85, 1.87 and 1.84 eV, respectively, larger than their E_g^{opt} (1.75, 1.78 and 1.72 eV, respectively). This discrepancy might have been caused by the presence of an energy barrier at the interface between the polymer film and the electrode surface; similar phenomena have been reported for other polymer systems.^[48,49]

Table IV-3. Optical absorption and electrochemical properties of 1T-BO20, 2T-BO20 and 3T-BO20.

Polymer	λ_{\max} (nm)	E_g^{opt} (eV)	HOMO (eV)	LUMO (eV)	E_g^{cv} (eV)
1T-BO20	608, 663	1.75	-5.53	-3.68	1.85
2T-BO20	611, 661	1.78	-5.32	-3.45	1.87
3T-BO20	602, 651	1.72	-5.34	-3.5	1.84

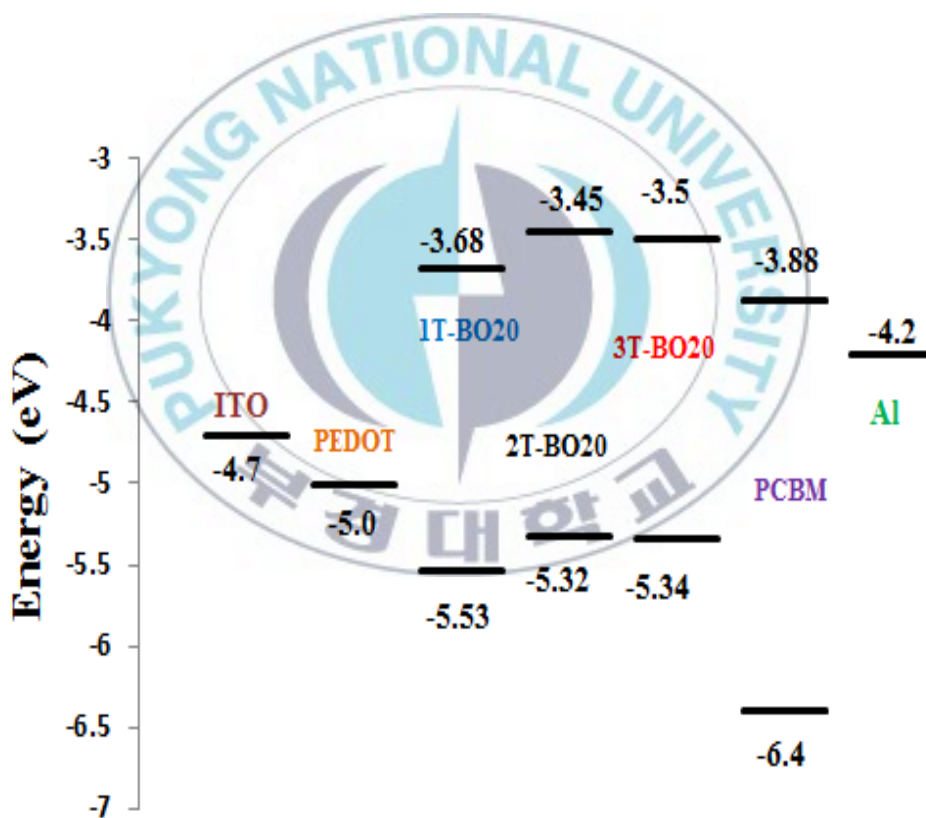


Figure IV-5. Energy level diagram of 1T-BO20, 2T-BO20 and 3T-BO20.

IV-3-4. Photovoltaic Properties

Broad absorption, appropriate HOMO/LUMO positions make 1T-BO20, 2T-BO20 and 3T-BO20 promising donor materials in BHJ OSCs. Therefore, the photovoltaic performances of these polymers were investigated in OSCs having the sandwich structure ITO/PEDOT:PSS/polymer:PC₆₁BM/Al. The photoactive layers have been spin-coated from solutions of the polymer and PC₆₁BM with different ratios and concentrations. It is known that solvents used for the preparation of the active layer have a strong impact on the performance of the cell. Here, we choose chloroform for the three polymers to obtain the films with the relatively good quality. The most efficient devices comprised a polymer/ PC₆₁BM ratio of 1:2 w/w with a polymer concentration of 5 mg/mL. In this case, we added a small amount of DIO used as a processing additive (1%, by volume relative to CF) to optimize the miscibility of the blends and morphology.

❖ *Devices without DIO*

Figure IV-6 shows the typical *J-V* curves of polymers:PC₆₁BM devices in the dark and under the illumination of AM 1.5G, 100 mW/cm². The corresponding V_{oc} , J_{sc} , FF, PCE of the devices are summarized in Table IV-4. The devices prepared from polymer:PC₆₁BM blends of 1T-BO20, 2T-BO20 and 3T-BO20 exhibited V_{oc} of 0.82, 0.82, and 0.73 V, respectively; each value is related to the

difference between the HOMO energy level of the polymer and the LUMO of PCBM. The device with 1T-BO20 exhibited a higher V_{oc} than 3T-BO20 which benefits from its lower-lying HOMO energy level. Surprisingly, devices based on 2T-BO20 and 1T-BO20 had the same V_{oc} value, even though 2T-BO20 has higher lying HOMO energy level. When 1T-BO20 compared to 3T-BO20, with increasing of thiophene rings in an acceptor moiety, J_{sc} increased. However, in the case of 2T-BO20-with increasing the thiophene ring in donor moiety, the J_{sc} decreased; even though absorption spectrum of 2T-BO20 is red-shift in comparison of 1T-BO20. This is probably due to the lower molecular weight of 2T-BO20 compared to 1T-BO20. It has been reported that the low efficiency of solar cells fabricated from low molecular weight polymers originates mainly from the reduced charge carriers mobility in the donor phase of the heterojunction.^[50] The J_{sc} values of the devices with the 1T-BO20, 2T-BO20 and 3T-BO20 films were 4.74, 3.39 and 4.98 mA/cm², respectively. The FF values of the devices based on 1T-BO20, 2T-BO20 and 3T-BO20 were 42.7, 61.5, and 52.8%, respectively, whereas the PCE values were 1.66, 1.71 and 1.92%, respectively. The highest PCE of 3T-BO20 could be due to higher J_{sc} and FF.

❖ *Devices with DIO*

Furthermore, when we incorporated DIO (1 vol %) into the 1:2 (w/w) polymer:PC₆₁BM blends, the device based on 1T-B020 exhibited significantly

increased J_{sc} , V_{oc} and FF of 8.37 mA/cm², 0.85 V and 48.0%, respectively, which lead to an enhancement of PCE from 1.66% to an outstanding value of 3.65 %. Besides, after adding DIO series resistance (R_s) of device decreased from 10.5 to 3.29 Ω .cm², whereas parallel (shunt) resistance (R_p) increased from 10.7 to 57.9 Ω .cm². This result revealed that DIO affected to control the morphology of active layer and it benefit for the exciton dissociation and carrier collection efficiency, thus leading to an increase in the short-circuit current density as well as the device efficiency.^[51] In the case of 2T-BO20, J_{sc} also increased from 3.39 to 5.55 mA/cm², V_{oc} was not changed and strangely, FF dropped from 61.5 to 52.8% even though R_s value decreased from 7.03 to 2.36 Ω .cm² and R_p value increased from 6.64 to 29.7 Ω .cm² compared to those of device without DIO. However, PCE of device with DIO also improved from 1.71 to 2.4%. Interestingly, we found that the polymer 3T-BO20, showed a very different response to the addition of DIO compared to 1T-BO20 and 2T-BO20. This polymer gave the best performances without adding any DIO. The J_{sc} and PCE of 3T-BO20 decreased to 4.3 mA/cm² and 1.76%, respectively. The low J_{sc} obtained for this polymer possibly due to the morphology not being fully optimized through adding DIO or 3T-BO20 has already reached the optimal morphology in the blend without DIO.

The change in J_{sc} possibly due to the changes in nanoscale morphology since DIO does not react with the polymer or fullerene and there is no DIO present in

the completely dried films.^[52] In order to investigate the effects of the additives on the surface morphologies, we measured the atomic force microscopy (AFM). Figure IV-8 shows the surface topography of BHJ films as directly measured from the same solar cell devices before and after the incorporation of DIO referred to in Figure IV-6 and IV-7, respectively. As shown in Figure IV-8 without adding DIO, the root-mean-square roughness (RMS) of the 1T-BO20/PC₆₁BM, 2T-BO20/PC₆₁BM and 3T-BO20/PC₆₁BM films were 7.48, 3.98 and 5.66 nm, respectively. However, when DIO was used, RMS values of the blend films increased to 10.72, 5.89 and 11.54 nm for the films of 1T-BO20/PC₆₁BM, 2T-BO20/PC₆₁BM and 3T-BO20/PC₆₁BM, respectively. The morphology of 1T-BO20/PC₆₁BM film processed with DIO (Figure IV-8b) showed larger scale phase separation and higher surface roughness than that in the BHJ film made without using processing additive. Because of the more optimized morphology, both of the polymers showed significant enhancement of J_{sc} and FF, which lead to an increase in PCE.^[51] In the case of 2T-BO20/PC₆₁BM blend film prepared from DIO, a significant reduction in phase separation and small domain size is observed in Figure IV-8d. The morphology of this blend film was more uniform than that of 2T-BO20/PC₆₁BM blend film without DIO. Besides, there is no large phase separation, showing good miscibility between 2T-BO20 and PC₆₁BM.^[53] This leads to a large interface for exciton dissociation and bicontinuous interpenetrating networks for free charge transportation, which is well consistent

with the improved J_{sc} in devices.^[54] In contrast, the blend film of 3T-BO20/PC₆₁BM with DIO (Figure IV-8f) exhibited rough film and much larger domain sizes with RMS surface roughness of 11.54 nm indicating large phase separation took place. The severe phase separation in active layer reduces the area for charge separation and increases the exciton diffusion length and the recombination of charges, leading to low photocurrent.



Table IV-4. Photovoltaic properties of OSCs incorporating BO-based polymers.

Active layer Polymer/ PC ₆₁ BM	Thickness (nm)	J_{sc} (mA/cm ²)	V_{oc} (V)	FF (%)	PCE (%)	R_s ($\Omega \cdot \text{cm}^2$)	R_p (k $\Omega \cdot \text{cm}^2$)
1T-BO20	150	4.74	0.82	42.7	1.66	10.5	10.7
1T-BO20^a	115	8.37	0.85	48.0	3.65	3.29	57.9
2T-BO20	125	3.39	0.82	61.5	1.71	7.03	6.64
2T-BO20^a	145	5.55	0.82	52.8	2.40	2.36	29.7
3T-BO20	120	4.98	0.73	52.8	1.92	9.06	11.2
3T-BO20^a	125	4.30	0.79	51.9	1.76	12.6	24.6

^a1% DIO was added to the active layer solution

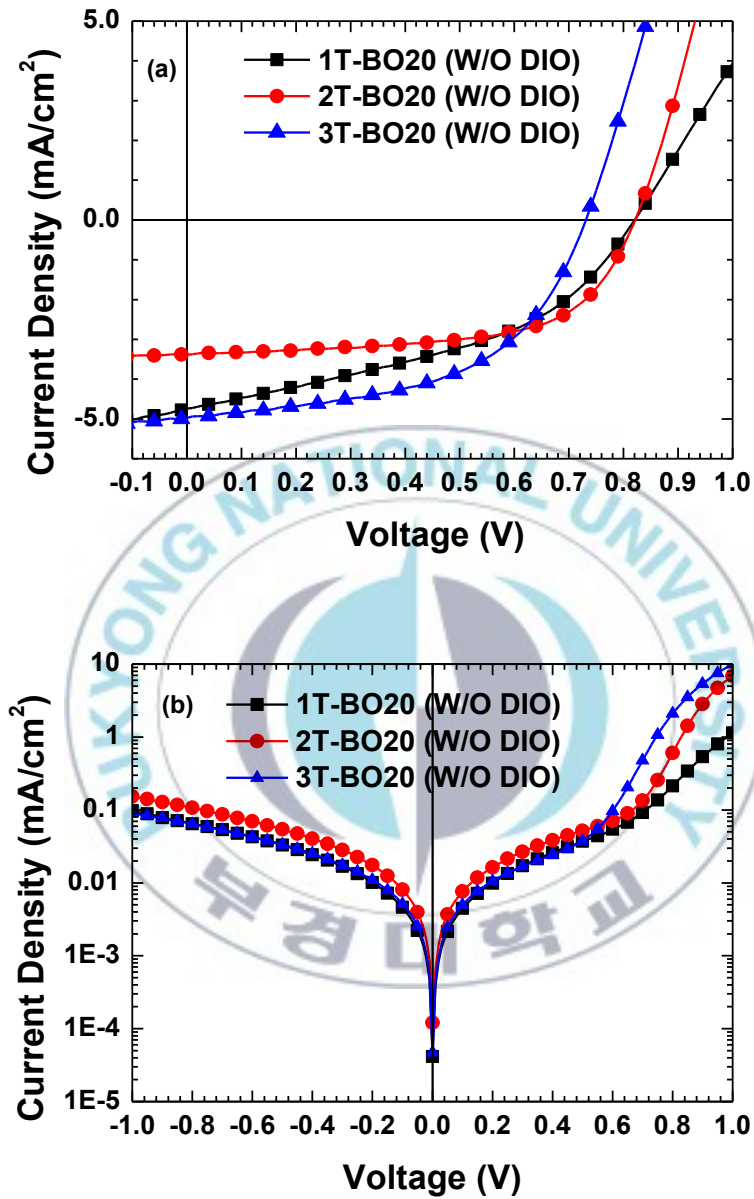


Figure IV-6. J - V curves of OSCs based on 1T-BO20, 2T-BO20 and 3T-BO20.

- c) Under the illumination of AM 1.5G, $100 \text{ mW}/\text{cm}^2$
- d) Under the dark condition

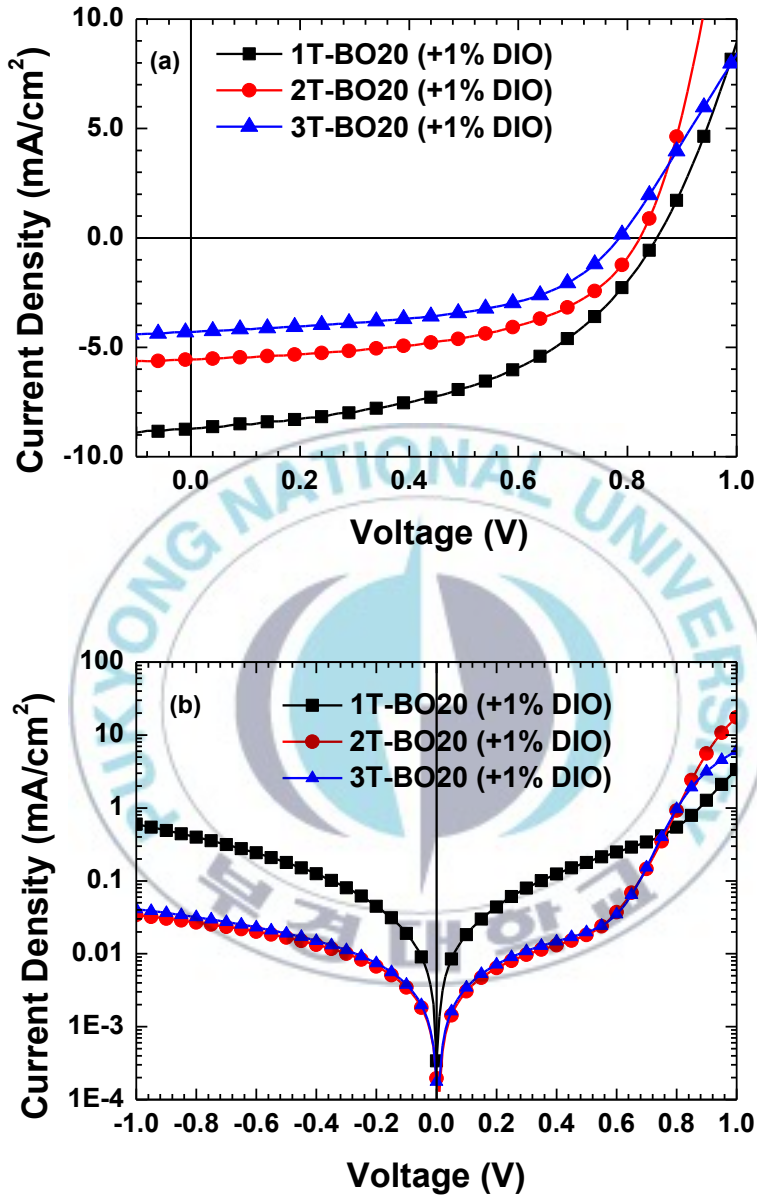


Figure IV-7. J - V curves of OSCs based on 1T-BO20, 2T-BO20 and 3T-BO20 with 1% DIO.

- c) Under the illumination of AM 1.5G, $100 \text{ mW}/\text{cm}^2$
- d) Under the dark condition

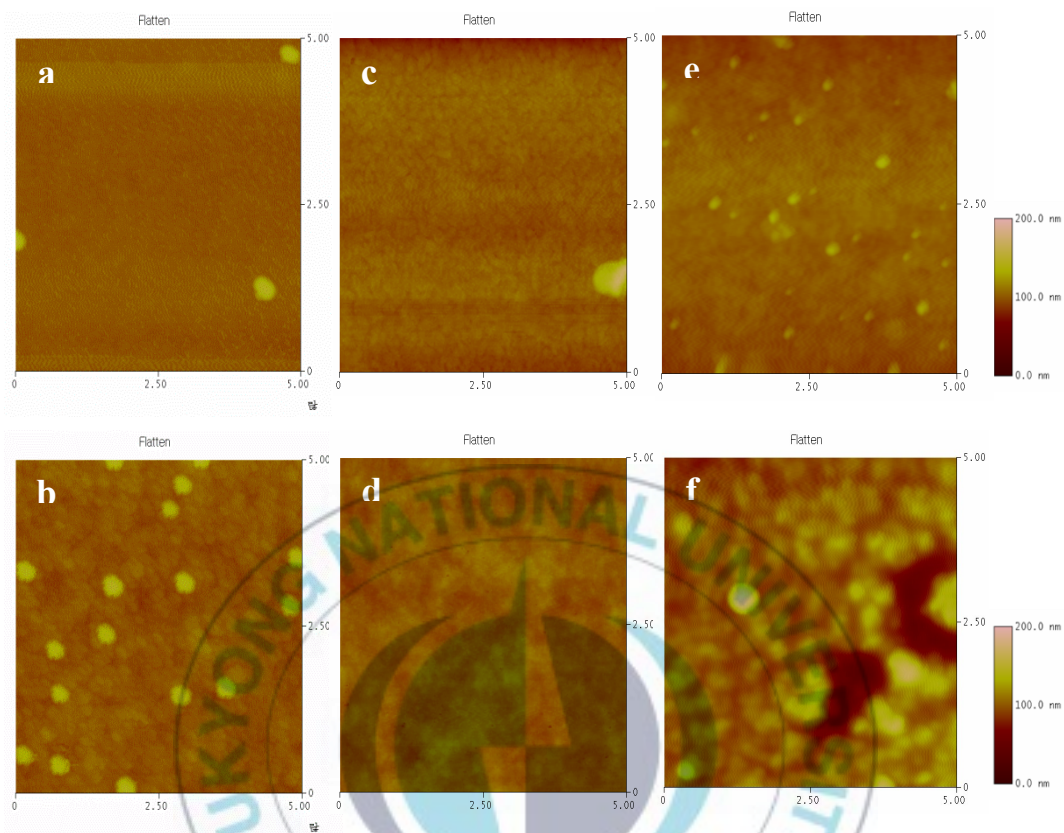


Figure IV-8. AFM height images of polymer:PC₆₁BM blend films: (a) 1T-BO20 without DIO; (b) 1T-BO20 with 1% DIO; (c) 2T-BO20 without DIO; (d) 2T-BO20 with 1% DIO; (e) 3T-BO20 without DIO; (f) 3T-BO20 with 1% DIO.

IV-4. Conclusion

Through the synthesis of polymers 1T-BO20, 2T-BO20 and 3T-BO20 based on 2,1,3-benzooxadiazole derivative we have demonstrated that the utility of various thiophene rings and their positions in the repeating unit affect to optical, electrochemical and photovoltaic properties of polymers. On other hand, we found that BHJ OSC devices prepared from blends of these polymers and PC₆₁BM processed with DIO showed very different responses. Both of polymers 1T-BO20 and 2T-BO20 based devices with DIO exhibited an enhancement of PCE from 1.66 to 3.65% and from 1.71 to 2.4%, respectively; whereas 3T-BO20 gave the best performance without adding any DIO. PCE of device based on 3T-BO20 reduced from 1.92 to 1.76% when adding 1% of DIO.

References

- [1] T. Kietzke (2001), *Advances in OptoElectronics*, **2007**, 1-15.
- [2] A. Mishra, and P. Bauerle (2012), *Angew. Chem. Int. Ed.*, **51**, 2020-2067.
- [3] B. C. Thompson, and J. M. J. Frechet (2008), *Angew. Chem. Int. Ed.*, **47**, 58-77.
- [4] T. M. Clarke, and J. R. Durrant (2010), *Chem. Rev.*, **110**, 6736-6767.
- [5] S. Gunes, H. Neugebauer, and N. S. Sariciftci (2007), *Chem. Rev.*, **107**, 1324-1338.
- [6] H. Hoppe, and N. S. Sariciftci (2004), *J. Mater. Res.*, **19**, 1924-1945.
- [7] H. Zhou, L. Yang, and W. You (2012), *Macromolecules*, **45**, 607-632.
- [8] B. Ratier, J. M. Nunzi, M. Aldissi, T. M. Kraft, and E. Buncel (2012), *Polym Int.*, **61**, 342-354.
- [9] C.J. Brabec (2004), *Solar Energy Materials & Solar Cells*, **83**, 273-292.
- [10] S. E. Shaheen, C. J. Brabec, N. S. Sariciftci, F. Padinger, T. Fromherz, and J. C. Hummelen (2001), *Appl. Phys. Lett.*, **78**, 841-843.
- [11] F. Zhang, K. G. Jespersen, C. Bjorstrom, M. Svensson, M. R. Andersson, V. Sundstrom, K. Magnusson, E. Moons, A. Yartsev, and O. Inganas (2006), *Adv. Funct. Mater.*, **16**, 667-674.
- [12] E. Hauff, J. Parisi, and V. Dyakonov (2006), *Thin Solid Films*, **511**, 506-511.
- [13] J. Nakamura, K. Murata, and K. Takahashi (2005), *Appl. Phys. Lett.*, **87**, 132105 1-3.

- [14] G. Li, V. Shrotriya, Y. Yao, and Y. Yang (2005), *J. Appl. Phys.*, 043704 1-3.
- [15] T. Y. Chu, J. Lu, S. Beaupré, Y. Zhang, J. R. Pouliot, J. Zhou, A. Najari, M. Leclerc, and Y. Tao (2012), *Adv. Funct. Mater.*, 201102623 1-7.
- [16] S. J. Lou, J. M. Szarko, T. Xu, L. Yu, T. J. Marks, and L. X. Chen (2011), *J. Am. Chem. Soc.*, **133**, 20661–20663.
- [17] J. K. Lee, W. L. Ma, C. J. Brabec, J. Yuen, J. S. Moon, J. Y. Kim, K. Lee, G. C. Bazan, and A. J. Heeger (2008), *J. Am. Chem. Soc.*, **130**, 3619 -3623.
- [18] H. Hoppe, and N. S. Sariciftci (2006), *J. Mater. Chem.*, **16**, 45-61.
- [19] M. M. Wienk, M. G. R. Turbiez, M. P. Struijk, M. Fonrodona, and R. A. J. Janssen (2006), *Appl. Phys. Lett.*, **88**, 153511 1-3.
- [20] J. Hou, M. H. Park, S. Zhang, Y. Yao, L. M. Chen, J. H. Li, and Y. Yang (2009), *Macromolecules*, **41**, 6012-6018.
- [21] Y. Li, and Y. Zou (2008), *Adv. Mater.*, **20**, 2952-2958
- [22] J. Kim, S. H. Park, J. Kim, S. Cho, Y. Jin, J. Y. Shim, H. Shin, S. Kwon, I. Kim, K. Lee, A. J. Heeger, and H. Suh (2011), *Journal of Polymer Science: Part A: Polymer Chemistry*, **49**, 369-380.
- [23] X. Hu, L. Zuo, W. Fu, T. T. L. Olsen, M. Helgesen, E. Bundgaard, O. Hagemann, M. Shi, F. C. Krebs, and H. Chen (2012), *J. Mater. Chem.*, **22**, 15710-1576.
- [24] H. Akpınar, A. Balan, D. Baran, E. K. Unver, and L. Toppare (2010), *Polymer*, **51**, 6123-6131.

- [25] I. Nurulla, A. Tanimoto, K. Shiraishi, S. Sasaki, and T. Yamamoto (2002), *Polymer*, **43**, 1287-1293.
- [26] Q. Peng, J. Xu, and W. Zheng (2009), *Journal of Polymer Science: Part A: Polymer Chemistry*, **47**, 3399-3408.
- [27] T. Yamashita, S. Yamada, Y. Yamazaki, and H. Tanaka (2009), *Synthetic Communications*, **39**, 2982-2988.
- [28] J. R. Kumar, J. Jawaharl, and D. P. Pathak (2006), *E-Journal of Chemistry*, **3**, 278-285.
- [29] A. Balan, D. Baran, G. Gunbas, A. Durmus, F. Ozyurt, and L. Toppare (2009), *Chem. Commun.*, 6768-6770.
- [30] E. Bundgaard, and F.C. Krebs (2007), *Sol. Energy Mater. Sol. Cells*, **91**, 954-985.
- [31] N. Blouin, A. Michaud, D. Gendron, S. Wakim, E. Blair, R. Neagu-Plesu, M. Belletete, G. Durocher, Y. Tao, and M. Leclerc (2008), *J. Am. Chem. Soc.*, **130**, 732-742.
- [32] R. T. Weitz, K. Amsharov, U. Zschieschang, E. B. Villas, D. K. Goswami, M. Burghard, H. Dosch, M. Jansen, K. Kern, and H. Klauk (2008), *J. Am. Chem. Soc.*, **130**, 4637-4645.
- [33] M. Zhang, X. Guo, Z. G. Zhang, and Y. Li (2011), *Polymer*, **52**, 5464-5470.
- [34] J. Y. Lee, K. W. Song, J. R. Ku, T. H. Sung, and D. K. Moon (2011), *Solar Energy Materials & Solar Cells*, **95**, 3377-3384.

- [35] J. Y. Lee, S. M. Lee, K. W. Song, and D. K. Moon (2012), *European Polymer Journal*, **48**, 532-540.
- [36] F. Babudri, S. R. Cicco, L. Chiavarone, G. M. Farinola, L. C. Lopez, F. Naso, and G. Scamarcio (2000), *J. Mater. Chem.*, **10**, 1573-1579.
- [37] J. Sleven, C. G. Walrand, and K. Binnemans (2001), *Materials Science and Engineering C*, **18**, 229-238.
- [38] C. Topaçli, A. Topaçli, M. Civan, F. Ercan, M. Durmu, and V. Ahsen (2008), *Thin Solid Films*, **516**, 8299-8306.
- [39] V. Wintgens, and C. Amiel (2004), *Journal of Photochemistry and Photobiology A: Chemistry*, **168**, 217-226.
- [40] C. J. Brabec, A. Cravino, D. Meissner, N. S. Sariciftci, T. Fromherz, M. T. Rispens, L. Sanchez, and J. C. Hummelen (2001), *Adv. Funct. Mater.*, **11**, 374-380.
- [41] M. C. Scharber, D. Muhlbacher, M. Koppe, P. Denk, C. Waldauf, A. J. Heeger, and C.J. Brabec (2006), *Adv. Mater.*, **18**, 789-794.
- [42] J. M. Jiang, P. A. Yang, T. H. Hsieh, and K. H. Wei (2011), *Macromolecules*, **44**, 9155-9163.
- [43] J. M. Jiang, P. A. Yang, H. C. Chen, and K. H. Wei (2011), *Chem. Commun.*, **47**, 8877-8879.
- [44] P. Ding, C. Zhong, Y. Zou, C. Pan, H. Wu, and Y. Cao (2011), *J. Phys. Chem. C*, **115**, 16211-16219.

- [45] B. Zhang, X. Hu, M. Wang, H. Xiao, X. Gong, W. Yang, and Y. Cao (2012), *New J. Chem.*, **36**, 2042-2047.
- [46] M. Helgesen, S. A. Gevorgyan, F. C. Krebs, and R. A. J. Janssen (2009), *Chem. Mater.*, **21**, 4669-4675.
- [47] P. Piyakulawat, A. Keawprajak, K. Jiramitmongkon, M. Hanusch, J. Wlosnewski, U. Asawapirom (2011), *Solar Energy Materials and Solar Cells*, **95**, 2167-2172.
- [48] D. A. M. Egbe, L. H. Nguyen, H. Hoppe, D. Muhlbacher, N. S. Sariciftci (2005), *Macromol. Rapid Commun.*, **26**, 1389-1394.
- [49] T. Yamamoto, B. L. Lee (2002), *Macromolecules*, **35**, 2993-2999.
- [50] S. E. Shaheen, C. J. Brabec, N. S. Sariciftci, F. Padinger, T. Fromherz, J. C. Hummelen (2001), *Appl. Phys. Lett.*, **78**, 841-843.
- [51] L. Dou, J. Gao, E. Richard, J. You, C. C. Chen, K. C. Cha, Y. He, G. Li, Y. Yang (2012), *J. Am. Chem. Soc.*, **134**, 10071-10079.
- [52] Y. Zhang, Z. Li, S. Wakim, S. Alem, S.-W. Tsang, J. Lu, J. Ding, Y. Tao (2011), *Organic Electronics*, **12**, 1211-1215.
- [53] Y. Liang, L. Yu (2010), *Acc. Chem. Res.*, **43**, 1227-1236.
- [54] Z. Ma, E. Wang, K. Vandewal, M. R. Andersson, F. Zhang (2011), *Appl. Phys. Lett.*, **99**, 143302-143303.

Acknowledgements

The help and continuous support from professors, classmates, friends, and family to whom I am most grateful, will never be forgotten. Without all of you, I would not be what I am today. I would like to thank each of you individually by word, but I do so in my heart.

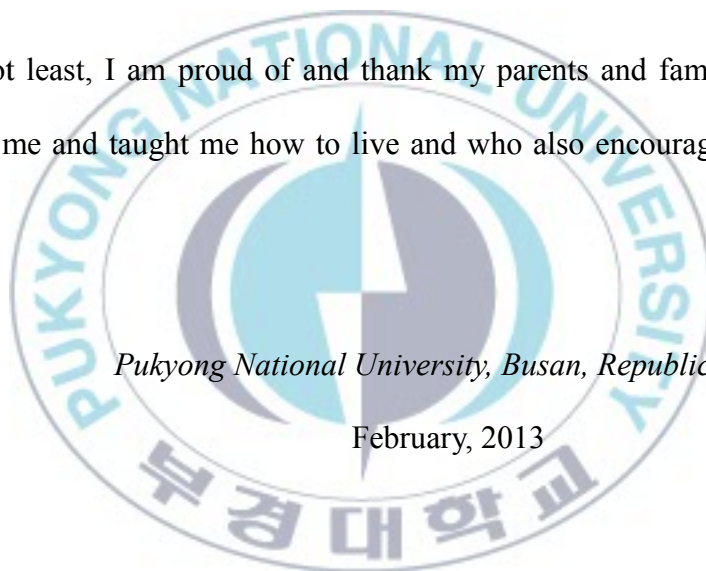
Foremost, I would like to express my sincere gratitude to my advisor Professor **Joo Hyun Kim** for the continuous support of my Master study and research, for his patience, motivation, enthusiasm, and immense knowledge. His guidance helped me in all the time of research and writing of this thesis. I could not have imagined having a better advisor and mentor for my Master study. He is not only my professor, but also my father. He always takes care and cheers me on.

I thank my fellow lab-mates in Organic Opto-electronic Materials Lab (OOM): Y. H. Bae, M. Y. Jo, D. S. Yoo, H. S. Hong, Y. E. Ha, J. H. Park, K. E. Im, J. H. Park for their inspiration to elevate my moral courage, care, the stimulating discussions, for the sleepless nights we were working together before deadlines, and for all the fun we have had in the last two years. They gave me a comfortable and active environment as well as enthusiastic and invaluable help during the time spent working with them. I also thank all Vietnamese students at Pukyong National University for their friendship and encouragement.

I am obliged to express my heart full thanks to all professors in Department of

Polymer Engineering: S. K. Min, C. Y. Park, S. B. Park, B. Lee, W. K. Lee, S. I. Yoo for knowledge, encouragement, insightful comments. I thank all professors at the Faculty of Chemical Engineering in Ho Chi Minh City University of Technology, who provided many engineering tools and background knowledge that I gained their classes. I also thank all officers at Department of Polymer Engineering. They help me to comply with all of the necessary formalities during my study.

Last but not least, I am proud of and thank my parents and family, who have looked after me and taught me how to live and who also encouraged me during my studies.



Pukyong National University, Busan, Republic of Korea

February, 2013

Do Thu Trang